ESC European Society of Cardiology

European Heart Journal - Cardiovascular Imaging (2022) **23**, 14–30
https://doi.org/10.1093/ehjci/jeab221

REVIEW

Left atrial evaluation by cardiovascular magnetic resonance: sensitive and unique biomarkers

Dana C. Peters [1,*], Jérôme Lamy[1], Albert J. Sinusas[2], and Lauren A. Baldassarre[2]

[1]Department of Radiology and Biomedical Imaging, Yale School of Medicine, New Haven, CT, USA; and [2]Department of Cardiology, Yale School of Medicine, New Haven, CT, USA

Received 3 August 2021; editorial decision 6 October 2021; accepted 12 October 2021; online publish-ahead-of-print 29 October 2021

Left atrial (LA) imaging is still not routinely used for diagnosis and risk stratification, although recent studies have emphasized its importance as an imaging biomarker. Cardiovascular magnetic resonance is able to evaluate LA structure and function, metrics that serve as early indicators of disease, and provide prognostic information, e.g. regarding diastolic dysfunction, and atrial fibrillation (AF). MR angiography defines atrial anatomy, useful for planning ablation procedures, and also for characterizing atrial shapes and sizes that might predict cardiovascular events, e.g. stroke. Long-axis cine images can be evaluated to define minimum, maximum, and pre-atrial contraction LA volumes, and ejection fractions (EFs). More modern feature tracking of these cine images provides longitudinal LA strain through the cardiac cycle, and strain rates. Strain may be a more sensitive marker than EF and can predict post-operative AF, AF recurrence after ablation, outcomes in hypertrophic cardiomyopathy, stratification of diastolic dysfunction, and strain correlates with atrial fibrosis. Using high-resolution late gadolinium enhancement (LGE), the extent of fibrosis in the LA can be estimated and post-ablation scar can be evaluated. The LA LGE method is widely available, its reproducibility is good, and validations with voltage-mapping exist, although further scan–rescan studies are needed, and consensus regarding atrial segmentation is lacking. Using LGE, scar patterns after ablation in AF subjects can be reproducibly defined. Evaluation of 'pre-existent' atrial fibrosis may have roles in predicting AF recurrence after ablation, predicting new-onset AF and diastolic dysfunction in patients without AF. LA imaging biomarkers are ready to enter into diagnostic clinical practice.

* Corresponding author. Tel: +1 203 737 6360. E-mail: dana.peters@yale.edu
Published on behalf of the European Society of Cardiology. All rights reserved. © The Author(s) 2021. For permissions, please email: journals.permissions@oup.com.

Graphical Abstract

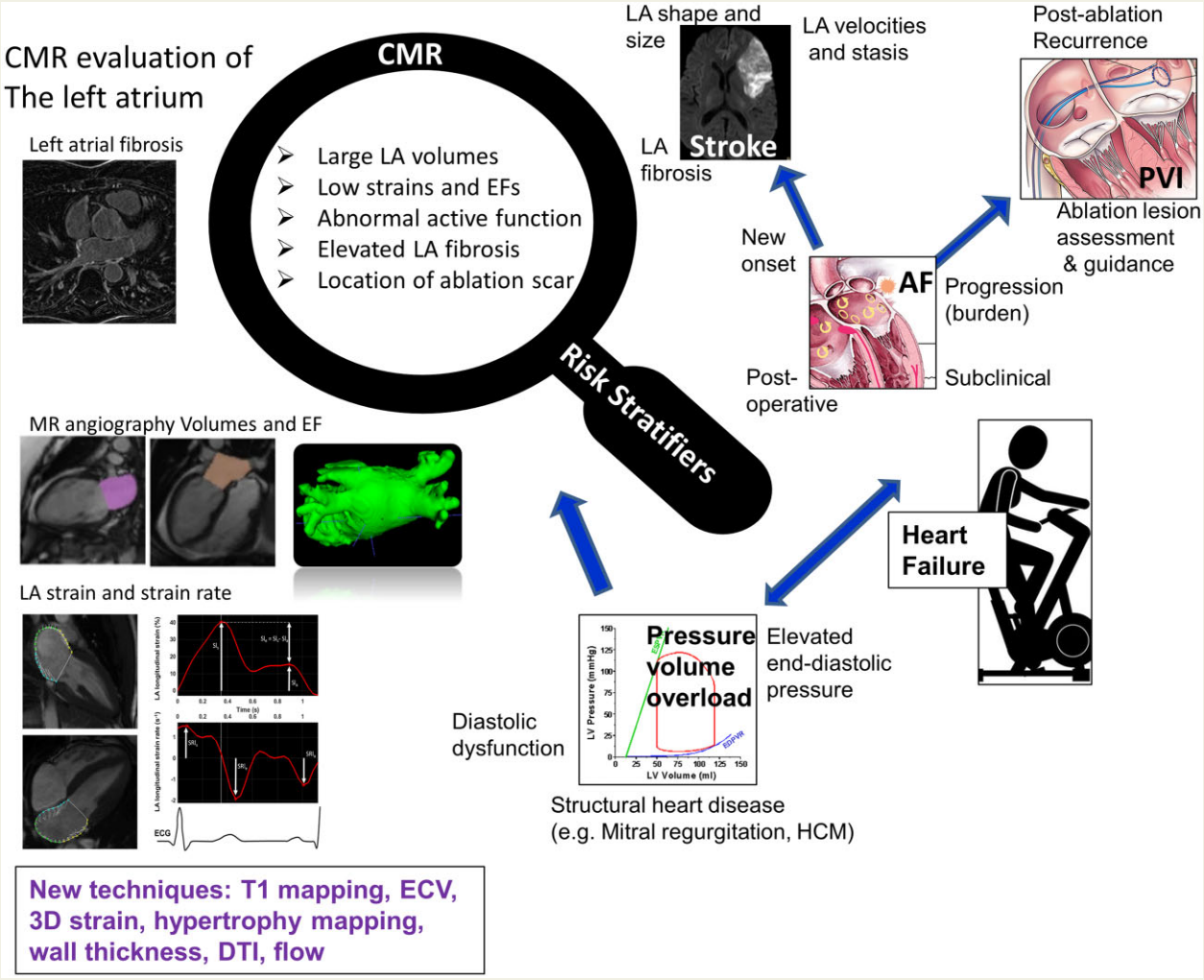

Keywords left atrium • cardiovascular magnetic resonance • strain • strain rate • volume • late gadolinium enhancement • fibrosis

Introduction

The left atrium (LA) is increasingly recognized as the bellwether,[1] whose characterization provides important prognostic information as a biomarker of subclinical disease,[2] reflecting diastolic dysfunction[3] and the presence of atrial fibrillation (AF). The LA remodels as it responds to higher left ventricular (LV) diastolic filling pressures.[4] Function of the LA is controlled by mitral valve plane motion in systole and the properties of LV relaxation in early diastole. Only at the end of the cardiac cycle, during the 'A-wave' does the LA myocardium contract (a.k.a. 'booster function or atrial kick'), finishing the work of LV filling (~20% of stroke volume under normal conditions). While LA remodelling (fibrosis, increased volume, reduced function among other forms) is most strongly associated with AF,[5] a highly common disease of chaotic electrical activity arising from the LA,[6] LA remodelling is present in a variety of cardiovascular diseases.

LA anatomy defined by MR angiography and cine

The anatomy of the LA as defined by cardiovascular magnetic resonance (CMR) imaging is shown in *Figure 1*. The pulmonary veins (PVs) (most often 4, but variants with 3–5 veins exist[7,8]) fill the LA with oxygenated blood from the lungs. The left atrial appendage (LAA) acts as a decompression chamber, but also as a location where thrombus can develop.[9] Anatomy can be defined with contrast-enhanced MR angiography (MRA). Contrast MRA typically uses 0.1–0.2 mmol/kg

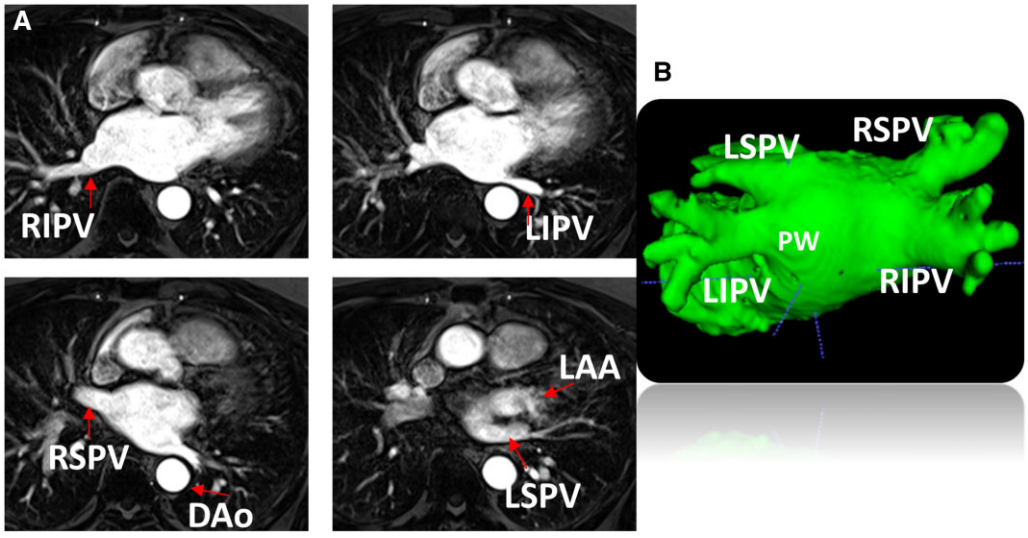

Figure 1 (*A*) Standard examples of slices from 3D contrast MR angiography, showing the pulmonary veins and shape and size of the left atrium. (*B*) 3D rendering of the left atrium, viewing the posterior wall.

gadolinium contrast agent and employs a breath-held dynamic time-resolved three-dimensional (3D) gradient echo sequence to acquire multiple phases during injection (4–8 s per phase), with typical spatial resolution of 1–2 mm^3, with 400 mm FOV, repetition time of 2–3 ms, and flip angle of 20–40°. The frame with greatest contrast opacification is typically analysed.[10,11] For acceleration of MR image acquisition, parallel imaging (factor 2) can be employed, plus partial Fourier and view-sharing methods such as 3D TRICKS.[12,13] The timing of the breath-hold relative to the injection can be determined using a bolus-timing scan.[14] Semi-automated segmentation software is commercially available for analysis of contrast MRA images of the LA.[15,16] Contrast MRA of the LA and PVs is commonly performed, for planning prior to pulmonary vein isolation (PVI) by ablation, where the number and size of the veins are useful, and the DICOM data are often imported into the advanced navigation software of an ablation system.[17] Electrocardiogram (ECG) gating is not used in MRA of the LA, although some recent approaches have demonstrated the possibility of ECG-gated non-contrast 3D balanced steady-state free precession (bSSFP) methods. bSSFP imaging of the LA and PVs is challenging, because of the blood flow from the highly off-resonant lung generates artefacts in bSSFP.[18] This is present but remains barely noticeable in conventional long-axis cine,[19] but prevents successful 3D bSSFP cine acquisitions. However, new approaches show promise for 3D ECG-gated non-contrast bSSFP based MRA.[20,21]

Analysis of morphological features (size, shape, sphericity, etc.) from 3D angiographic images of *LA and LAA* derived using both magnetic resonance imaging (MRI)[22,23] and CT[24–27] have been shown to be predictive of stroke, AF, and AF recurrence after PVI. Although not all studies using these shape-marker findings have consistently replicated the prognostic value.[25]

While 3D MRA is used for planning ablation procedures, two-dimensional (2D) cine is commonly used to measure *LA volumes and evaluate global LA function* (ejection fraction, EF). The conventional technique is shown in *Figure 2*, in which the two-chamber and four-chamber cine are acquired and the area is planimetered, either manually or using semi-automated tools[28,29] available on many software platforms. Some studies have been performed using Simpson's method with a dedicated LA short-axis stack,[30,31] or use of two-, three-, and four-chamber views.[32] Correlations between values derived by bi-plane and Simpson's methods are strong.[33] Phasic measurement of volumes is useful for evaluating atrial booster function, but even measurement of minimum and maximum volume yields important information. Volume at any point in the cardiac cycle is measured on long-axis cine by planimetered areas ($Area_{2Ch}$ and $Area_{4Ch}$), and the long-axis length (L) measurements (see *Figure 2*), using the bi-plane formula, informed by echocardiographic recommendations:[34]

$$V = 0.85\,\frac{(Area_{2Ch} \cdot Area_{4Ch})}{Length}.$$

Normal values are 38 ± 11 mL/m^2, 14 ± 5 mL/m^2, and 50–62 ± 8% for maximum, minimum volume, and total EF.[35] An excellent recent summary[35] notes that several areas of non-standardization in volume measurement exist. These include how to measure length (use of averaged value or the smaller value or length from two-chamber only acquisitions), and whether and how to include the PVs and LA appendage (most exclude). Minimum and maximum LA volumes and total LA EF do not change greatly with age, and thus are sensitive markers of disease, but active LA EF increases with age (reflecting mild diastolic dysfunction).[30,36] Women have smaller LA volumes, although this difference disappears after indexing by body surface area.[36] More data are needed on normal values for active function (but see[37]) which requires careful phasic measurement, and might have greater predictive power, e.g. in hypertrophic cardiomyopathy (HCM).[38] LA EF is more powerful than LV EF in predicting heart failure outcomes.[39] A major pitfall in evaluation of LA volumes and function is the use of long-axis images that are suboptimal due to

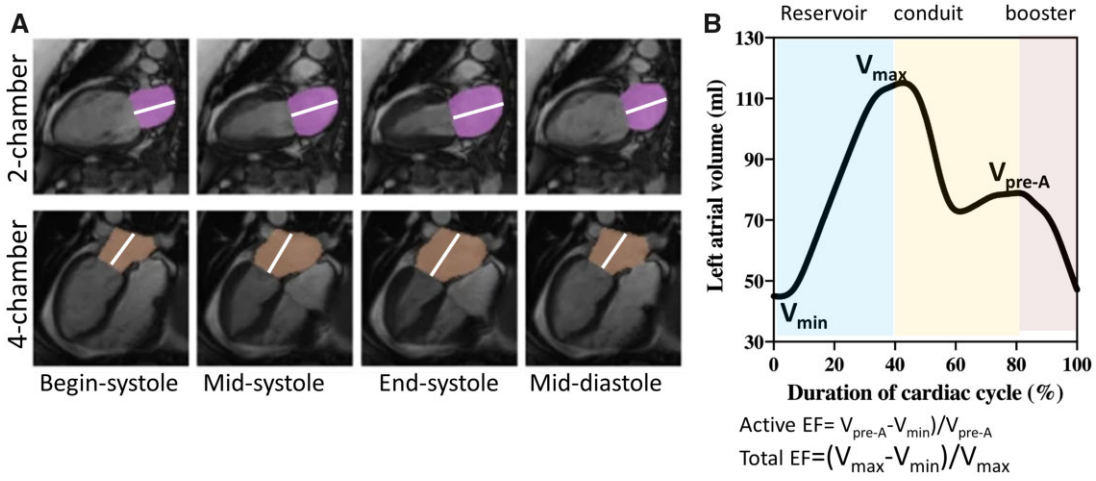

Figure 2 (*A*) LA volume and ejection fraction assessment, using two-chamber and four-chamber views, with areas and lengths planimetered. (*B*) LA volume vs. time curve, showing three characteristic volumes, V_{min}, V_{max} and V_{pre-A} for evaluation.

incomplete presentation of the LA (i.e. 'foreshortening'). If employed, inaccurate values of volume and function will be measured[40] and the test–retest reproducibility will be poor.

LA strain and strain rate

Myocardial strain analysis is a relatively recent method to evaluate LA function. Expressed as percentage, strain illustrates the relative deformation of the myocardium. Usually computed in the longitudinal direction of the LA, it can be expressed as a Lagrangian strain: $Sl(t) = (L(t) - L_0)/L_0$, with $L(t)$ the length of a myocardial segment at time t of the cardiac cycle and L_0 the initial length of the segment, initialized at the QRS complex of the ECG. Strain is complemented by its derivative, the strain rate, an expression of the deformation rate of the LA. The LA strain and strain rate curves are available along the full cardiac cycle and allow a complete evaluation of the LA function and the extraction of indices characteristic of the different atrial phases (see *Figure 3*): (i) LA peak reservoir strain (Sls) (with 'l' denoting longitudinal, 's' denoting systole) after filling to maximal volume prior to the mitral valve opening in end-systole, (ii) LA booster pump strain (Sla), 'a' denoting atrial contraction phase, when LV filling is completed in late diastole, and (iii) the LA strain in the conduit phase (Sle = Sls - Sla) ('e' denoting emptying phase) corresponding passive emptying in early diastole. Strain rate peaks are evaluated as the maximal strain rate magnitudes during: (i) the LA filling in mid-systole (SRls), (ii) the LA emptying in early diastole after the mitral valve opens (SRle), and (iii) the LA contraction completing the LV filling in late diastole (SRla). Typical normal values for peak strain (%) and strain rate (%/s) are Sls of 30.6 ± 10.6, SRls of 1.29 ± 0.51;[41] or Sls of 25.0 ± 5.4, SRls of 1.2 ± 0.4.[42]

Tissue tracking was technically developed in the 90s,[43,44] but the success of LV myocardial tagging methods prevented popularization of this approach with MRI. Meanwhile, LA strain by tagging was not possible, due to the thin LA myocardium, and at that time it was not a metric of interest. Early LA strain evaluations were done using echocardiographic tissue Doppler imaging[45] or by speckle tracking.[46] Similarly, the first strain analyses from MRI standard cine images were inspired by speckle tracking and used block matching tissue tracking for the LV[47,48] and were later extended to the LA.[37,49,50] To date, tissue tracking methods applied to long-axis cine images are the only relevant methods for LA strain quantification, as specific magnetization tagging sequences are unable to evaluate the thin LA myocardium.

MRI tissue tracking for LA strain evaluation involves post-processing of routinely acquired two- and four-chamber cine bSSFP images during the full cardiac cycle. Several packages allow evaluation of LA strain, based on either optical flow-related methods like block matching (2D CPA MR (TomTec Imaging Systems[48]) Multimodality Tissue Tracking (Toshiba[41]) CardioTrack[51] or non-rigid image registration.[52] Other available packages likely also follow one of those two categories (CVI 4.2 Tissue Tracking software) [e.g. Circle Cardiovascular Imaging, MR-Wall Motion Tracking software (Vitrea, Canon Medical Systems), QStrain (Medis Medical Imaging Systems)]. Tissue tracking process is usually semi-automatic and the user is required to initialize the LA contour in two- and four-chamber views; initialization is required at a single time frame (maximal or minimal volume). Strain is by definition strongly related to LA volume and EF, but might also reflect stiffness or fibrosis. 3D tissue tracking analysis based on 3D cine of the LA is an important area of development.[53,54]

LA strain pathophysiology

LA strain has been shown to be capable of detecting subclinical changes related to normal physiological conditions; with a global decrease in LA strain indices with ageing, slightly lower LA function values in men compared to women and differences between races.[42,55,56] While MRI studies tend to confirm echocardiography findings, the sub-field is relatively new and population studies are sparse.[42,56,57]

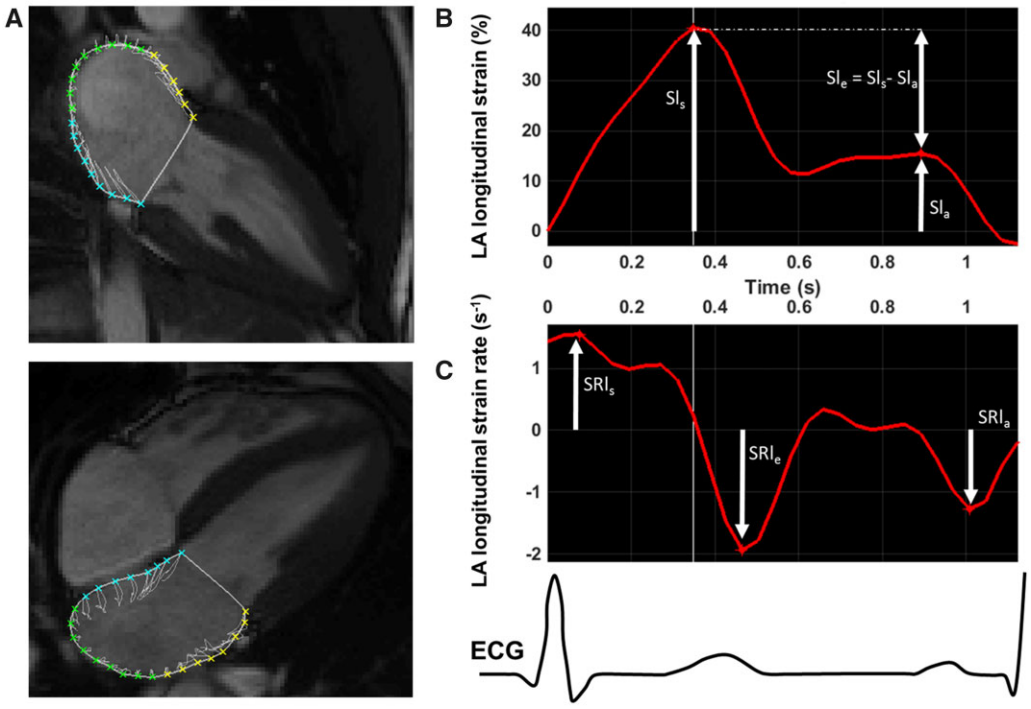

Figure 3 (*A*) LA strain is evaluated by contouring the 2ch and 4ch throughout the cardiac cycle to calculating regional deformation. (*B*) The strain plotted over the cardiac cycle exhibits a characteristic pattern, and peak global longitudinal strain in systole (Sls), emptying strain (Sle = Sls - Sla) and active strain (Sla) can be measured. (*C*) The time derivative of the strain curve provides strain rates, with important peaks in LV systole (SRls) and early (SRle) and late diastole (SRla).

LA strain has power as an excellent non-invasive early prognostic and diagnostic aid beyond simple LA size alone.[58–61] Decreased LA strain is a stronger predictor of cardiovascular events compared to LA EF or LA indexed volume.[62,63] A recent large study of the general population from Multiethnic Study of Atherosclerosis (MESA) reported an association of decreased LA strain indices by MRI in subjects with cardiovascular risk factors.[56] Also in the general population, LA strain predicts new cardiovascular events.[64]

Indications of LA remodelling based on decreased peak reservoir strain, even when LA size is normal, has been described in cardiometabolic diseases like hypertension[65–67] and diabetes.[65,68] Besides onset of new AF, LA strain has also been able to predict AF recurrence after ablation,[69,70] and post-operative AF after cardiac valve surgery.[71] LA strain also provides, in some cohorts, efficient grading of diastolic dysfunction[72] and was able to evaluate precisely the LV filling pressure elevation.[73] LA strain is also considered as a non-invasive surrogate for tissue remodelling and has been shown to decrease with the extent of tissue replacement evaluated by histology[74,75] and by LGE evaluation.[76,77]

Commonly, only peak LA strain in systole (Sls, also called 'global longitudinal strain') is reported. While other strain or strain rate magnitudes seem to evolve along the same trajectory as Sls, they may hold other information. Indeed, while LA strain is known to be load dependent,[78] this is less the case for strain rate indices. Moreover, recent studies promote the evaluation of the peak booster function strain, which may hold complementary information. Increasingly, studies show that LA booster pump peak strain is a more intrinsic marker of the LA function, e.g. changing to compensate for loss of LV filling during the LA conduit phase in early remodelling stages like in obesity[79] and indicating subclinical AF.[80]

Reproducibility, normal values, and limitations

MRI tissue tracking LA strain analyses from routinely acquired cine SSFP long-axis images have shown excellent inter-exam and inter-operator reproducibility[51,81–83] and modest to excellent inter-vendor and inter-modality (echo vs. MR) agreement.[84] Since, as in echocardiography,[85] strong variations of LA strain indices between the different vendors remain, this limits the use of absolute LA strain normal values.[84] Normal values for MRI-cine LA strain exist for normal to low-risk ageing populations.[42,56,57,83] Optimal spatial and temporal resolutions of cine SSFP images for LA strain MRI tissue tracking are still unknown despite preliminary work in this area for the LV.[50,86] Finally, as in echocardiography, the LA is easily foreshortened, and then, just as for LA EFs, this leads to overestimated strain values.[40,87,88]

LA late gadolinium enhancement

LA LGE can be used to evaluate fibrosis associated with remodelling, due to either pressure or volume overload, that is present in many cardiomyopathies and thought to be the 'arrhythmic substrate' of AF. It can also evaluate acute or chronic scar caused by ablation after a PVI procedure. The earliest histology studies found that atrial fibrosis was implicated in AF.[89] Histology data showed that in patients with mitral regurgitation and AF, there was greater amount of fibrosis compared to age-matched patients with regurgitation but no AF.[90] It is now recognized that many diseases, including mitral regurgitation, HCM,[91] and structural heart disease[92] result in atrial fibrosis, prior to the onset of clinical AF, based on histological analyses and confirmed by MR imaging.[93,94] The mechanisms for this remodelling are well categorized by others.[95] The first *in vivo* mapping of this atrial fibrosis was performed by electrophysiology voltage mapping of the atrium in AF patients.[96] These maps found regions of low-voltage, which was equated with fibrosis. At the same time, the development of late gadolinium enhancement (LGE) methods emerged,[97,98] which was used to evaluate fibrosis and scar. MRI is currently unequalled in the ability to delineate fibrotic tissue, based on increased extra-cellular volume fraction (ECV), and this is especially useful in the LV. LGE was quickly adapted for use in evaluating *atrial* fibrosis and scar.[99]

Acquisition and technical considerations

LGE[97] is a method that uses bolus injection of gadolinium contrast agent (usually 0.2 mmol/kg dose), and then images the contrast enhancement later during the equilibrium phase, 10–30 min after injection (thus the name LGE). At this juncture, the contrast agent is distributed throughout the body, in vascular and in extra-cellular spaces (~25% of myocardial space), but excluded from intact myocytes. In myocardial regions with more extra-cellular matrix (fibrosis), more contrast agent is able to enter, thus the bulk contrast concentration is higher, and therefore the myocardial T1 shortens.[100] With abject scar from infarction or ablation, or even diffuse fibrosis associated with remodelling, ECV increases (from normal values of ~25% up to ~85% for replacement scar),[101] which is reflected in higher contrast concentration and T1 shortening of the myocardium post-injection. LV fibrosis can be imaged using a T1-weighted ECG-gated inversion recovery sequence, with segmented gradient echo readout.[97] LA LGE[99] uses this same technique, but modified in several ways (*Figure 4* and *Table 1*), mainly driven by a need for greater contrast (between fibrosis and blood and fat), and higher spatial resolution to visualize scar in the thin atrial wall (~2 mm).[102] 3D LA LGE sequence is available on most scanners with excellent results (*Figure 5*).

3D LA LGE, like 2D LV LGE, requires user input of *the inversion time* (TI, see *Figure 4*). In LV LGE, often two R-Rs between inversions are used, in conjunction with phase-sensitive inversion recovery (PSIR),[103] to perform a phased reconstruction that is somewhat immune to poor TI choice. For 3D LA LGE, one R-R interval (1RR) between inversions is employed, since doubling scan time is infeasible. For the 1R-R LA LGE, a 1R-R TI-scout should be used. The TI at which the LV myocardium is nulled, plus a 'fudge factor' (60 ms at our institution) provides a good TI choice. Automated TI estimation based on heart rate, scan protocol, and current myocardial T1-value is possible.[104] Navigator-gated implementations of PSIR for 3D LGE have been developed, and do show utility, although it is critical that both the first and second heart-beat both be (independently) respiratory-gated.[105] The myocardial T1 and therefore optimal TI does drift upward over 5 min, but only slightly (<10 ms),[106] and is not a concern. 3D LGE can only detect atrial fibrosis with a signal higher than blood (i.e. T1 shorter than blood's). Therefore, LA LGE must begin >15 min after injection, at which point contrast between blood and fibrosis is significant:[106] even later is better (*Figure 6B*). A rule of thumb is that, if mitral valvular enhancement (*Figure 5A*) is not observed, the LA LGE is not analysable. Most contrast agents work similarly, although an agent whose concentration remains high in the blood pool longer is less effective,[107] since contrast between blood and scar is lower (and a lower dose must be used). Thus, LGE methods that generate darker blood and increase contrast have been proposed[108] and some have been tested for imaging the LA.[109]

The use of navigator (NAV)-gating provides *respiratory compensation* by monitoring the right hemi-diaphragm in real-time, to acquire data selectively during end-expiration. This increases the available scan time for data acquisition from 20 s breath-hold to ~2–4 min (4–8 min assuming 50% respiratory-gating efficiency). Prospective tracking of the LA is not used, and the tracking factor for the LA motion relative to the diaphragm has not been well characterized. It is essential that the 'phase-encoding direction', normally placed on axial images anterior–posterior, be set in the right-left direction. If not, chest wall ghosting (especially contrast-enhanced skin) will appear prominently, since the chest wall moves out of sync with the superior–inferior respiratory motion of the heart (*Figure 6A*). Use of a leading NAV (see *Figure 4*) in an inversion recovery sequence requires an NAV restore pulse (also shown in *Figure 4*), which reinverts the inverted right hemi-diaphragm, to preserve the diaphragmatic signal for monitoring respiration. Because this 'restore' pulse also reinverts PV blood, it generates a most problematic artefact, NAV-induced inflow artefacts, especially in the right PVs (see *Figure 5A*). Several approaches have been proposed to circumvent this artefact. Most easily implemented, the NAV can be acquired after the data acquisition segment (trailing NAV, see *Figure 4*) thus obviating the need for an NAV restore pulse (practically speaking this might require the technologist to eliminate the NAV restore pulse manually). Other strategies include an NAV acquired ~100 ms prior to data acquisition segment[110] that does not need an NAV restore, and use of an NAV restore pulse <180°,[111] which also reduces the inflow artefact. Even bellows-respiratory-gating works satisfactorily.[112]

Fat-saturation is essential, as fat encases the LA and has a short T1 (~210 ms). Indeed epicardial LA fat is a biomarker correlated to AF burden, AF recurrence, and new-onset AF,[113] and harbours the ganglionated plexi.[114] Fat suppression uses an SPIR (110° flip angle) and centric acquisition. Fat suppression with SPAIR (inversion of the fat, and linear acquisition of data) cannot succeed, because the fat—inverted by the prior 180°—has a very low signal prior to acquisition (see *Figure 4B*), so inversion is not an option (unless a fat restore pulse is used[115]) Dixon fat–water separation methods have been used with linear k-space acquisition order.[116]

Since many patients imaged with LA LGE have AF, a large minority of these patients are imaged during atrial *arrhythmia*, which results in an irregular RR interval, and no atrial kick. Interestingly, LA LGE quality is sometimes still good. However, quality is more often poor (*Figure 6C*), and this manifests as poor nulling of 'normal' LV

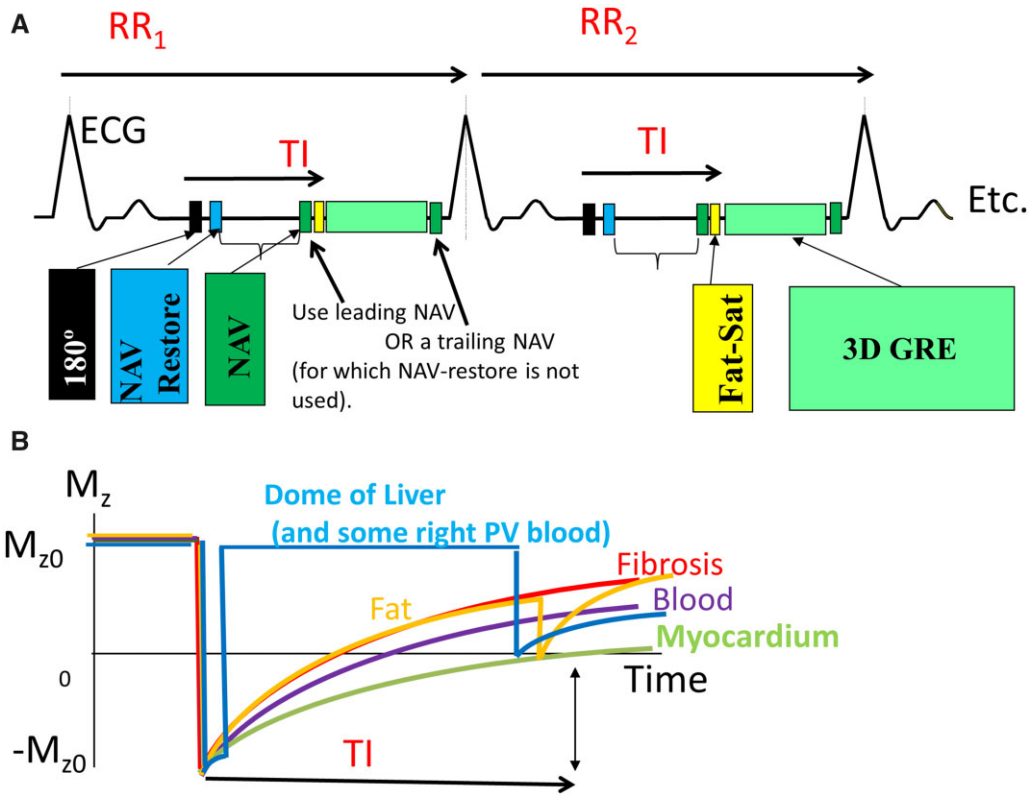

Figure 4 (*A*) The LA LGE pulse sequence uses an inversion recovery 3D GRE, with navigator-gating, fat-saturation and ECG gating. A 180° inversion pulse is used, with imaging performed at the inversion time (TI) shown when myocardium is nulled. Just before the 3D GRE acquisition, fat-saturation and the NAV pulses are applied. (*B*) Schematic of magnetization. Blood myocardium and scar are inverted, and imaging is performed when myocardium is nulled, at which time fibrosis is enhanced, relative to blood and myocardium, just as in 2D LGE. Fat is inverted too, and is not fully recovered after a time TI, but can be suppressed with a saturation pulse. The dome of the liver, used for navigator-gating is inverted too, so must be immediately reinverted with a NAV restore, so that at the time of the NAV pulse, the liver signal is high (alternatives exist, e.g. a trailing NAV–see diagram).

Table 1 Modifications of LV LGE sequence for use in 3D LA LGE

2D LV LGE	3D LA LGE
2D, Standard cardiac views	3D, axial, covering LA
1–2 × 1–2 × 6–8 mm^3	1–1.5 × 1–1.5 × 2–4 mm^3
TR/θ = 4–5 ms/15–20°	TR/θ = 4–5 ms/15–20°, zero-filling
Breath-hold, 10–20 s	Navigator-gated, 3–6 min
No fat-sat, sequential order	Fat suppression, centric order
1 or 2 RR between IR, TI from scout or use of PSIR	1RR between IR, TI from scout
Phase-encoding AP	Phase-encoding RL
Parallel imaging ×2	Parallel imaging ×2
10–30 min post-injection	15–30 min post-injection
Diastole, segmented GRE (~150 ms)	Diastole, segmented GRE (~150–200 ms) or systole (esp. in AF)
Scar signal is 3–6 SDs above myocardium or use FWHM method	Scar signal is 2–3 SD's above blood signal, or use IIR >1.4, or subject specific method

2D, two-dimensional; 3D, three-dimensional; GRE, gradient recalled echo, IIR, image intensity ratio; IR, inversion recovery; LGE, late gadolinium enhancement; LV, left ventricular; PSIR, phase-sensitive inversion recovery; RL, right-left; RR, R-R interval; SD, standard deviation; TI, inversion time; TR, repetition time.

myocardium, and ghosts, both problems due to variable time between RR intervals and thus inversion pulses, resulting in variable magnetization in each data acquisition.[104] Approaches to reducing these artefacts include a dynamic TI[117] or a dynamic saturation pulse,[104,118] both of which depend on the history of RR intervals, and use MR physics modelling to change the acquisition in real-time. However, these are not commercially available. Cardiac motion blurring is also a factor; imaging during LV systolic rest-period (LA

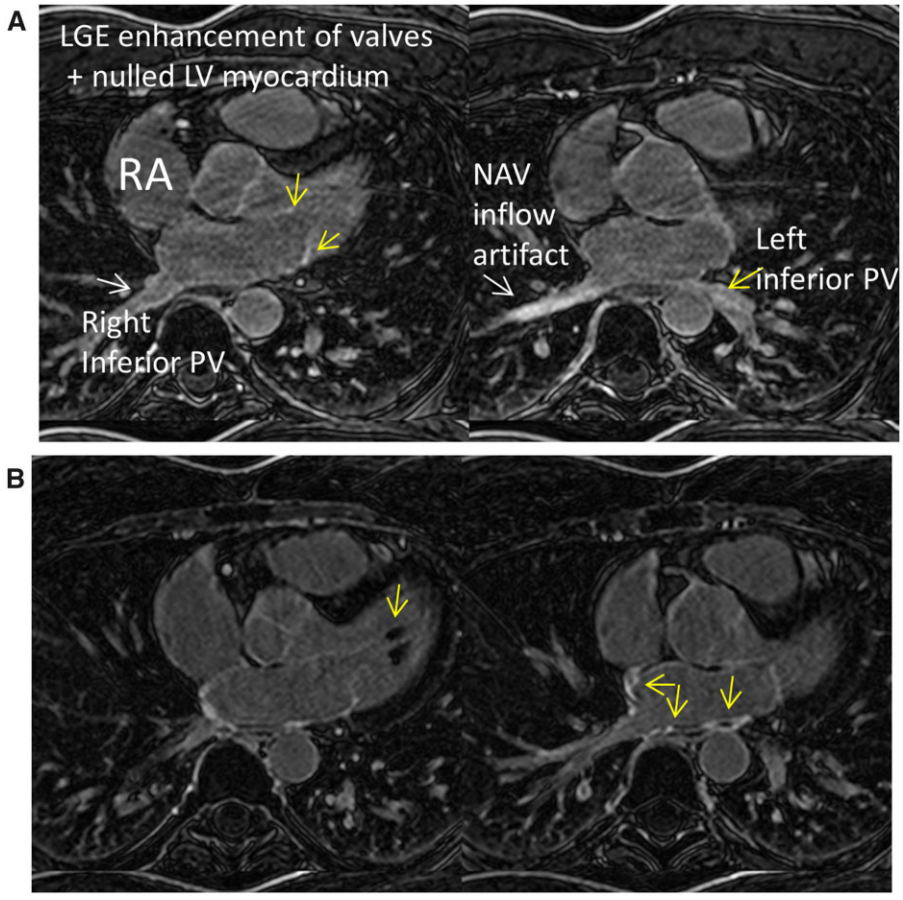

Figure 5 Pre- (*A*) and post-ablation (*B*) images (two slices in a single subject) exhibit important characteristics of LA LGE. (*A*) Valves should appear enhanced (yellow arrows, A), and myocardium should appear dark. Aortic wall also usually enhances. Fat is suppressed. The NAV artefact is apparent in this study (white arrow, A), and methods to remove it should be considered, and this artifactual enhancement must not be included as 'fibrosis'. (*B*) A good quality study will exhibit sharp features such as papillary muscles well delineated (arrow, B). After ablation, scar is clearly visible (arrows, B).

diastole) might help.[119] Finally, on average the signal-to-noise ratio (SNR) of LA LGE in patients with arrhythmia is inherently lower. This is because patients with greater AF burden have a slightly higher myocardial diffuse fibrosis,[120] thereby requiring a slightly shorter TI to null myocardium; surprisingly, this can impact SNR significantly.[104]

A study of factors in optimization of 3D LA LGE showed delayed imaging post-injection (and lower contrast dose) improved quality.[121] Alternative acquisition strategies such as spiral[122] and radial with variable under-sampling and compressed sensing reconstruction[123,124] have been studied for 3D LA LGE, although their role in improving quality is not established.

Utility of LA LGE

3D LA LGE was first introduced at as a method to identify *post-ablation scar*.[99] If able to identify gaps in ablation, this approach could inform 'redo' procedures and improve our understanding of why AF recurrence after PVI occurs. The value of this approach in identifying gaps in ablation sets has been investigated, but with conflicting results[125,126] for guiding an ablation procedure. Some found that simple extent of scar predicted freedom from recurrence, while others did not.[127–129] However, significant relationships with recurrence were found, i.e. less ostial scar in reconnected PVs,[127] or more scar around the right inferior PV.[128] Gaps in LA LGE have been compared to contact force made during ablation.[130] One recent study[131] found that electrical reconnection 3 months after ablation was found to be very common, by electrical mapping and LGE. There was a linear relationship between scar burden and extent of PV electrical reconnection. However, there was moderate location by location correspondence. Some lesion gaps may be non-conducting (and therefore not culprits in recurrence) and some apparently circumferential scar might have a gap large enough to conduct. Furthermore, possibly not all lesions are transmural, even in the very thin LA wall.[132] Furthermore, recurrence often is identified with electrical activity from a site not targeted for ablation.[133] Acute atrial ablation lesions can be imaged peri-procedurally using LA LGE, and T1- and T2-weighted imaging.[134–137]

Very early, 3D LA LGE was pioneered to identify *'pre-existent' atrial fibrosis*.[138] The concept that AF patients with highly remodelled atria are less easily cured with ablation and would more readily develop recurrent AF, led to a series of studies[139,140] by the Utah group to show

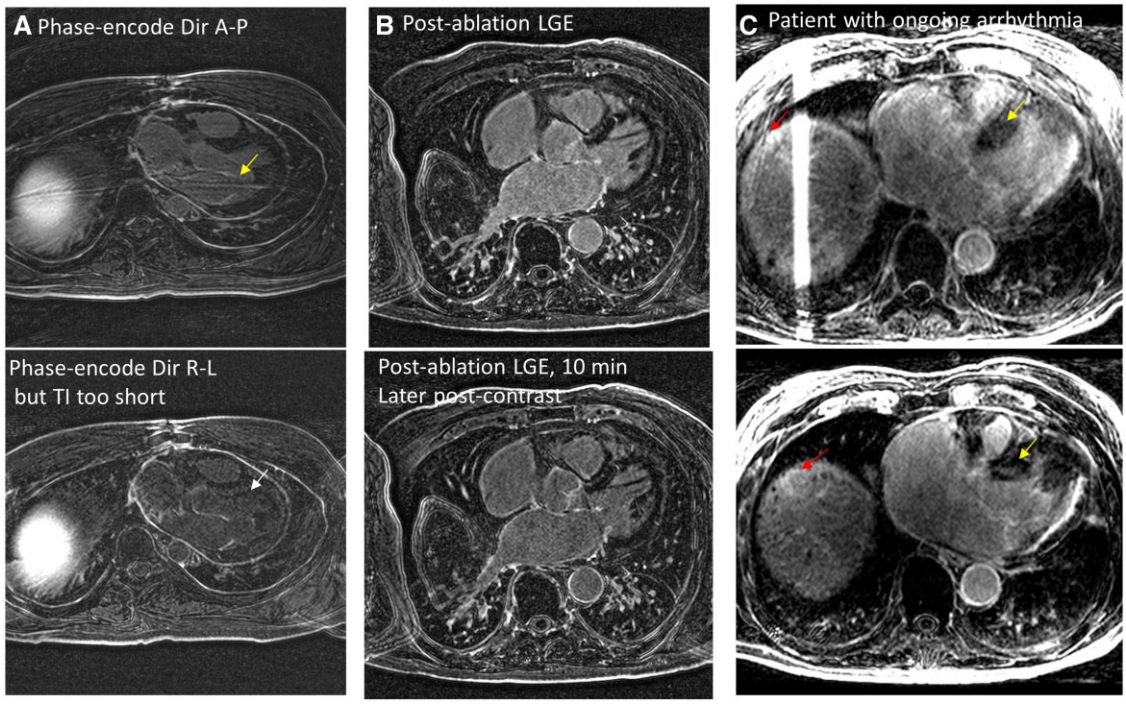

Figure 6 (*A*) Phase-encoding direction was chosen A-P, causing artefacts (yellow arrow). A repeat scan used phase-encoding R-L, so artefacts are removed, but TI was too short (white arrow). (*B*) A good quality post-ablation LA LGE image, repeated 10 min later shows improved contrast and greater conspicuity of scar. (*C*) LA LGE image of a patient with arrhythmia during scan exhibits poor nulling (yellow arrow) and diffuse artefacts (red arrow). A repeat scan using dynamic saturation pulses improved quality.

the predictive power of LA LGE. The DECAAF study involved 272 patients imaged prior to ablation for AF, followed for more than a year, and was able to improve prediction of recurrence using atrial fibrosis 'Utah stage', compared to clinical variables, with C statistic increasing from 0.65 to 0.69.[141] A follow-up trial will determine whether ablation of pre-existent scar improves PVI efficacy.[142] This finding has been partly replicated in studies from separate groups,[127,143,144] who found that patients with AF recurrence after PVI had significantly greater pre-existent scar. The hypothesis that AF is caused by rotors or re-entrant electrical activity in the LA, often anchored by fibrosis, has led some to compare fibrosis to rotors theoretically;[145,146] however, the experimental studies have not found a consistent relationship between rotor location and LA LGE thus far.[147,148] In a large retrospective studies of AF subjects, greater LA fibrosis was associated with stroke, both existing[149] and new onset.[150]

Increasingly, the concept of an 'atrial cardiomyopathy' has found support[151,152] from CMR studies. Atrial fibrosis is present to some degree in all people,[153] and especially present in those with a variety of cardiovascular diseases, from mitral regurgitation (where it might be expected due to pressure/volume overload), to HCM,[91] to subjects with coronary artery disease, to those with amyloid[154] or heart failure,[143] in addition to patients with AF. The concept that 'AF begets AF',[155] i.e. that atrial fibrosis develops mainly during AF, may be true, but atrial fibrosis often precedes atrial arrhythmias. In patients without AF, studies have shown that the extent of atrial fibrosis is associated with diastolic dysfunction.[156] Furthermore, the extent of fibrosis predicts new-onset atrial arrhythmias,[94] and even subclinical arrhythmias as shown in a large prospective trial.[157] A small but unique study[158] showed that patients without AF showed progression of LA LGE (from 13% to 18% in ~2 years), with both baseline LA LGE and extent of progression showing potential to indicate new-onset AF.

Controversies: thresholding, validation, and reproducibility

Early controversy suggested that LA LGE is not robust and noted that many cardiac structures enhanced (aortic wall, valve leaflets, and the atrium), so enhancement was non-specific. In fact, although not well recognized by the CMR community, these structures, the aortic wall (the tunica media[159]), and the valve[160] have significant extracellular matrix and enhance by LGE.

Table 2 summarizes reproducibility studies for LA LGE and average values, including scan–rescan studies, and reproducibility based on inter- and intra-observer variability in fibrosis segmentation for the same scan. Scan–rescan studies of post-ablation atrial LGE show good reproducibility,[129,165] with Sørensen–Dice (Dice) coefficients of up to 50–70% for ablation scar, in studies repeated at 2 days and 3 months. Such scan–rescan studies have not been performed in pre-ablation patients, which is a major gap in understanding.

Regarding the reproducibility of the segmentation of LA LGE, even more is known.[94,129,161,163,167,168] Dice overlaps of scar are often 40–50% pre-ablation and 70–80% post-ablation. These may seem to be modest value for Dice, but the sparsity of scar itself drives the Dice

Table 2 Fibrosis and post-ablation scar: reproducibility and values in disease groups and controls

Study first author and year	LGE extent/reproducibility	Disease	Age, % male, number of subjects	Comments
Quail *et al.* (2019)[94]	Intra-observer (bias ± 2 SDs): 0.3% ± 2.9%, ICC = 0.94 Inter-observer (bias ± 2 SDs): 0.6% ± 7.3%, ICC = 0.71 Mean pre-existent LGE 4.6%± 7.3%	AF and other CVD, pre-ablation	53 years old, 59%, *N* = 136	Variable threshold based on mitral valve signal, ∼CNR with blood >3
Habibi *et al.* (2014)[49]	5.8 ± 4.4% (Parox) vs. 9.2 ± 7.3% (persistent)	54 Parox AF 36 pers. AF	Age: 61 ± 10 years, 76%, *N* = 90	IIR > 1.6, no reproducibility data
Cochet *et al.* (2015)[161]	Intra-observer (bias ± 2 SDs): 0.1% ± 4.1% ICC = 0.96 Inter-observer (bias ± 2 SDs): 0.4% ± 5.4% ICC = 0.93 Mean pre-existent LGE 18.4 ± 8.9%	AF + other CVD	54 ± 4 years old, 65%, *N* = 190	Variable threshold Corview, CARMA
Bertelsen *et al.* (2020)[162]	Intra-observer (bias ± 2 SDs): -1.0 ± 2.8% ICC = 0.99 Inter-observer (bias ± 2 SDs): -1.7% ± 8.5% ICC = 0.96 Mean pre-existent LGE 2.8% (1.3–8.3) healthy, 9.0% (3.9–12.0) lone AF 20.1% (10.2–35.8) (older, no AF)	Healthy, lone AF, and older non-AF subjects	Healthy: 37 ± 6, 82%, *N* = 11 Lone AF: 39 ± 5, 91%, *N* = 11. Older, non-AF: 76 ± 5, 55%, *N* = 11	Galgo software, IIR = 1.2
Oakes *et al.* (2009)[163]	Pre-existent Mean LGE 17.1 ± 14.2% Inter-observer (bias ± 2 SDs) -0.9% ± 7% Intra-observer: (bias ± 2 SDs) 0.5 ± 5.5%	AF 51% parox	63.6 ± 12.0. 64%, *N* = 81	Variable threshold ∼3 SDs, Corview, CARMA
Malcolme-Lawes *et al.* (2013)[127]	∼3.5% pre-ablation ∼13% post-ablation	Parox AF	59.6 ± 13, 62%, *N* = 50	No reproducibility data
Khurram *et al.* (2014)[164]	Local IIR thresholds of >0.97 and >1.61 corresponded to bipolar voltage <0.5 and <0.1 mV, respectively	AF, 56% parox, mixed pre-ablation (43%) and post-ablation (57%)	62 ± 8.3 old, 75%, *N* = 75	IIR
Chubb *et al.* (2018)[129]	Mean post-ablation LGE ∼25% Scan–rescan (bias ± 2 SDs) -1% ± 10%, ICC = 0.7–0.8	Post-ablation AF Compared studies 2 days apart	61± 9, 78%, *N* = 40	Post-ablation AF Compared studies 2 days apart
Kamali *et al.* (2020)[165]	Scan-recan study post-ablation: Dice ∼74% (Otsu) Dice ∼64% (CNR > 3.3) Dice ∼56 % (IIR > 1.6)	3 months post-ablation, scan with rescan 3 months later	69.2 ± 12.0, 69%, *N* = 45	Used Otsu, IIR > 1.6 and CNR > 3.3
Benito *et al.* (2017)[166]	Post-ablation 14.5% (4.88–22.13) LGE = 1–2% for parox and perm AF	10 healthy subjects and 30 AF subjects pre- and post-ablation	Healthy: 22, 50%, *N* = 10 AF: 58 ± 10, 90%, *N* = 30	Used >1.3 IIR *R* = 0.2 for voltage vs. IIR Galgo
Karim *et al.* (2013)[167]	Pre-ablation Dice ∼45%, post-ablation Dice 75%. Bias +2 SDs: 1–3 ± 2–6 mls (pre-ablation) and 3–5 ± 4–8 mls post-ablation	30 pre-ablation and 30 post-ablation (AF)		Segmentation algorithms vs. expert consensus

AF, atrial fibrillation; CNR, contrast to noise ratio; Dice, Sørensen–Dice coefficient; ICC, intraclass correlation coeffciient; IIR, image intensity ratio; LGE, late gadolinium enhancement; SD, standard deviation.

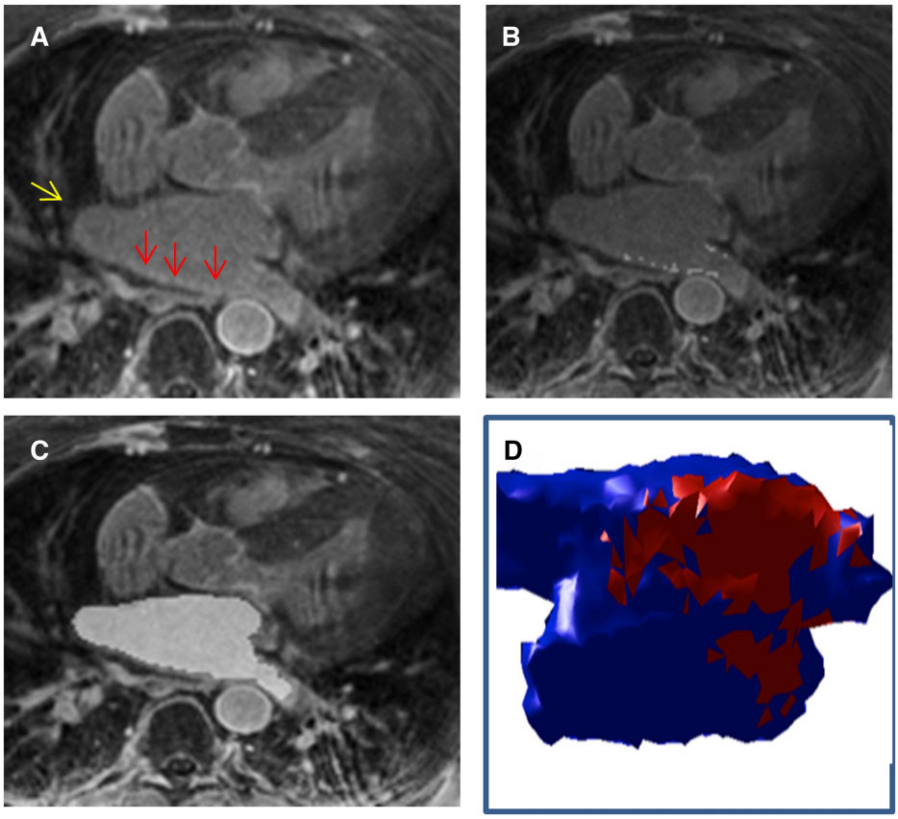

Figure 7 Segmentation of LA LGE. (*A*) Slice from LA LGE volume, with some enhancement regions of the atrial wall. (*B*) After thresholding, LA LGE is identified—excluding the enhanced signal of the mitral valve. (*C*) Segmentation of the LA cavity. (*D*) 3D reconstruction of LA LGE, and quantification of LA LGE volume in mls, can be performed.

metrics lower, compared to that reported, e.g. for the LV cavity. Inter and intra-observer agreement is good, even using study-specific thresholds, with low bias (near zero) and narrow limits of agreement (4–7%) on scar extent.[94,161]

Histological validation of LA LGE is mainly lacking, compared to LV LGE, where there has been comparison of LGE to histopathology of chronic infarct models.[98] In one study of 10 surgical ablation patients, agreement between Masson's Trichrome stain and LGE presence was observed, although statistical comparisons were not reported.[140] A study of ablation in the right atrium of pigs (left atrium is harder to access, requiring an atrial septal puncture) found that LA LGE thresholds of 2.3 standard deviations (SDs) above blood pool signal (acutely) and 3.3 chronically correlated best with histology.[169] Lacking animal models of AF, LA LGE has mainly been validated by comparison to surrogate markers. LA LGE extent has found consistent correlations with LA volume and EF,[94] LA strain,[76] CHADS(2) score,[149] age,[161] AF burden,[170] and presence of types of heart disease, including HCM, AF, and MR.[94,161] These relationships are typically not strong. The most relevant surrogate may be voltage mapping.

Voltage mapping has been used to validate LA LGE. Khurram *et al.*[164] found that a signal >1.6 image intensity ratio (IIR) corresponded to voltage <0.1 mV. Malcolme-Lawes *et al.*[127] found that LA LGE defined as >3 SDs above blood pool collocated to regions of lower voltage (<1 mV) on both pre-existent fibrosis and post-ablation scar. The relationship was moderate, which likely reflects reality. Others suggest that a threshold of 1.3 IIR identifies post-ablation scar best.[166]

LA LGE is segmented (*Figure 7*) by including enhanced signal located on the atrial wall. Subject-specific thresholds (e.g. based on mitral valve[94] or Otsu threshold[165]) or fixed thresholds, based on blood intensity and SD of signal in the blood pool (see *Table 2*) have been utilized. Thresholds that are advocated include signals >3 SDs above blood signal (CNR > 3) and signal 1.2–1.6 higher than blood signal (so-called IIR > 1.2–1.6). One scan–rescan study found that subject-specific Otsu threshold (using an atrial wall signal histogram) performed well.[165] *Figure 8* illustrates differences of these inter-related thresholds.[171] An IIR of 1 (i.e. a CNR of 0), sometimes advocated, is not practical, as it implies that half the atrium will be categorized as fibrotic even in the case where no fibrosis exists, since normal (partial-volumed) atrial wall is approximately isointense with the blood. The best thresholding approach would estimate ECV based on T1 mapping[172] for each study, and use as a standard threshold an ECV cut-off such as 55%. For example, based on analysis of LGE signal vs. T1, assuming a blood T1 of 300 ms, an IIR threshold of 1.4 (equivalent to a CNR of 3 if blood SNR of 7.5, see *Figure 8*), would identify atrial fibrosis with ECV >∼55%.[171]

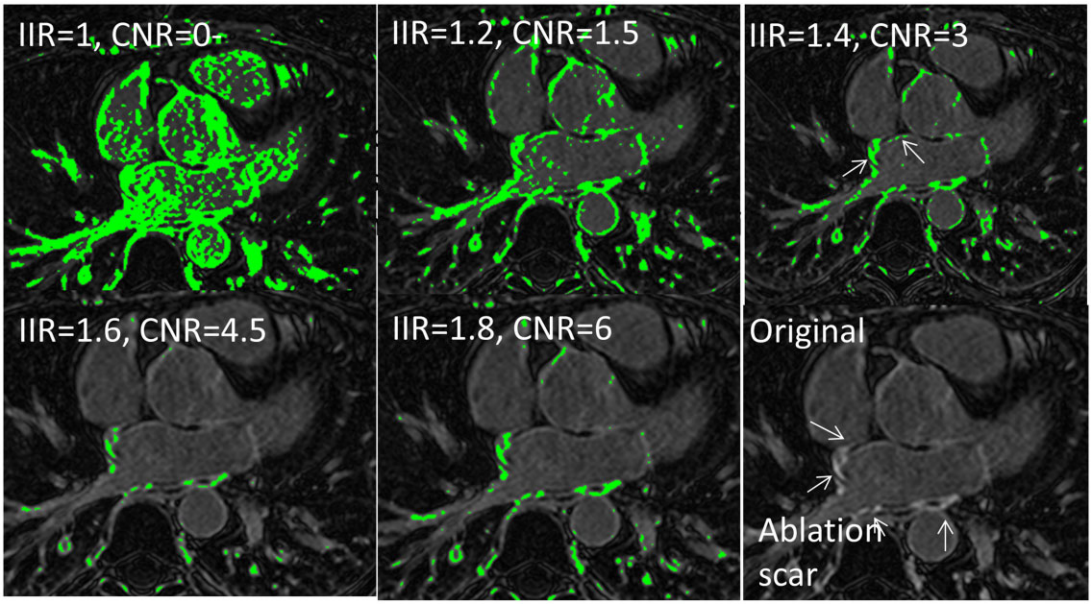

Figure 8 A single slice from a 3D LA LGE of a post-ablation subject is segmented with multiple thresholds (here shown as both image intensity ratio, IIR and CNR). IIR (vs. blood) and CNR above blood signal are two inter-related metrics for setting thresholds for segmenting fibrosis. They are linked since CNR = (IIR - 1)·SNR_b. Use of a threshold which is too low (e.g. IIR = 1.2) yields non-specific segmentation, while too high a threshold (e.g. IIR = 1.6) misses scar.

Another pitfall in segmentation relates to the identification of the atrial wall. PV sleeves are sometimes completely omitted from segmentations and enhanced mitral valve annular tissue (*Figure 5A*) is sometimes included as 'atrial fibrosis'. The LA LGE volume is often normalized by the LA myocardial volume (i.e. using a measurement of LA surface area multiplied by the LA wall thickness). The optimality of this normalization has not been explored. The LGE expressed in percent is also often log transformed for improved statistical testing (closer to normal distribution).

Future directions

Several *machine-learning networks* have been developed and validated to replace tedious manual segmentation of atrial volume and atrial scar on 3D LGE.[173–175] Limitations are that there is no consensus regarding the optimal scar thresholds and the definition of atrial wall, as noted above. This variability of expert segmentations and non-standardization is problematic for automated segmentation approaches for atrial fibrosis. Still this approach is highly valuable.

Echocardiography has shown that stasis of LA and LAA flow are important in thrombus formation.[176] LA and LAA flow can be measured with *four-dimensional (4D) phase contrast*; the earliest study documented the presence of vortical flow in the atrium, which it hypothesized is a method of conserving kinetic energy until needed during diastolic filling.[177] Later MR studies have been performed to document blood stasis, especially in patients with AF.[178–180] Mean and peak velocities in the LA were lower for AF vs. controls, while LA volumes were much greater. Such findings of stasis have been confirmed by other groups.[181] Other studies have compared 4D flow metrics to CHA2DS2-VASc score.[182] The reproducibility of 4D flow is reasonable for application to the LA.[183]

Diffusion tensor imaging, challenging even in the LV, has been performed in the atria, but only in ex-planted hearts.[184] Myocyte hypertrophy, a common pathological finding in the myocardium,[151] would be a useful imaging biomarker.[185] LA wall thickness measurement might be possible.[21] 3D strain maps are feasible and would add value. LA LGE would benefit from standardization and consensus regarding segmentation methods, automated analyses, further scan–rescan studies in pre-existent fibrosis, and strategies for stronger validation. Atrial contraction function may soon be more greatly utilized, as its evaluation is now more automated. In conclusion, LA imaging biomarkers are ready to enter into routine diagnosis and prediction!

Conflict of interest: none declared.

Funding

National Institutes of Health, HL155992.

References

1. Douglas PS. The left atrium—a biomarker of chronic diastolic dysfunction and cardiovascular disease risk. *J Am Coll Cardiol* 2003;**42**:1206–7.
2. Alfuhied A, Kanagala P, McCann GP, Singh A. Multi-modality assessment and role of left atrial function as an imaging biomarker in cardiovascular disease. *Int J Cardiovasc Imaging* 2021;doi: 10.1007/s10554-021-02316-x.
3. Rosenberg MA, Manning WJ. Diastolic dysfunction and risk of atrial fibrillation: a mechanistic appraisal. *Circulation* 2012;**126**:2353–62.
4. Mandoli GE, Sisti N, Mondillo S, Cameli M. Left atrial strain in left ventricular diastolic dysfunction: have we finally found the missing piece of the puzzle? *Heart Fail Rev* 2020;**25**:409–17.
5. Burstein B, Nattel S. Atrial fibrosis: mechanisms and clinical relevance in atrial fibrillation. *J Am Coll Cardiol* 2008;**51**:802–9.

6. Haissaguerre M, Jais P, Shah DC, Takahashi A, Hocini M, Quiniou G *et al.* Spontaneous initiation of atrial fibrillation by ectopic beats originating in the pulmonary veins. *N Engl J Med* 1998;**339**:659–66.
7. Porres DV, Morenza OP, Pallisa E, Roque A, Andreu J, Martinez M. Learning from the pulmonary veins. *Radiographics* 2013;**33**:999–1022.
8. Hauser TH, Yeon SB, McClennen S, Katsimaglis G, Kissinger KV, Josephson ME *et al.* A method for the determination of proximal pulmonary vein size using contrast-enhanced magnetic resonance angiography. *J Cardiovasc Magn Reson* 2004;**6**:927–36.
9. Manning WJ, Weintraub RM, Waksmonski CA, Haering JM, Rooney PS, Maslow AD *et al.* Accuracy of transesophageal echocardiography for identifying left atrial thrombi—a prospective, intraoperative study. *Ann Intern Med* 1995;**123**:817–22.
10. Francois CJ, Tuite D, Deshpande V, Jerecic R, Weale P, Carr JC. Pulmonary vein imaging with unenhanced three-dimensional balanced steady-state free precession MR angiography: initial clinical evaluation. *Radiology* 2009;**250**:932–9.
11. Fink C, Ley S, Kroeker R, Requardt M, Kauczor HU, Bock M. Time-resolved contrast-enhanced three-dimensional magnetic resonance angiography of the chest—combination of parallel imaging with view sharing (TREAT). *Invest Radiol* 2005;**40**:40–8.
12. Korosec FR, Frayne R, Grist TM, Mistretta CA. Time-resolved contrast-enhanced 3D MR angiography. *Magn Reson Med* 1996;**36**:345–51.
13. Schonberger M, Usman A, Galizia M, Popescu A, Collins J, Carr JC. Time-resolved MR venography of the pulmonary veins precatheter-based ablation for atrial fibrillation. *J Magn Reson Imaging* 2013;**37**:127–37.
14. Earls JP, Rofsky NM, DeCorato DR, Krinsky GA, Weinreb JC. Breath-hold single-dose gadolinium-enhanced three-dimensional MR aortography: usefulness of a timing examination and MR power injector. *Radiology* 1996;**201**:705–10.
15. Tobon-Gomez C, Geers AJ, Peters J, Weese J, Pinto K, Karim R *et al.* Benchmark for algorithms segmenting the left atrium from 3D CT and MRI datasets. *IEEE Trans Med Imaging* 2015;**34**:1460–73.
16. Depa M, Sabuncu MR, Holmvang G, Nezafat R, Schmidt EJ, Golland P. Robust atlas-based segmentation of highly variable anatomy: left atrium segmentation. *Lect Notes Comput Sc* 2010;**6364**:85–94.
17. Malchano ZJ, Neuzil P, Cury RC, Holmvang G, Weichet J, Schmidt EJ *et al.* Integration of cardiac CT/MR imaging with three-dimensional electroanatomical mapping to guide catheter manipulation in the left atrium: implications for catheter ablation of atrial fibrillation. *J Cardiovasc Electrophysiol* 2006;**17**:1221–9.
18. Hu P, Stoeck CT, Smink J, Peters DC, Ngo L, Goddu B *et al.* Noncontrast SSFP pulmonary vein magnetic resonance angiography: impact of off-resonance and flow. *J Magn Reson Imaging* 2010;**32**:1255–61.
19. Robb JS, Hu CX, Peters DC. Interleaved, undersampled radial multiple-acquisition steady-state free precession for improved left atrial cine imaging. *Magn Reson Med* 2020;**83**:1721–9.
20. Aouad P, Koktzoglou I, Milani B, Serhal A, Nazari J, Edelman RR. Radial-based acquisition strategies for pre-procedural non-contrast cardiovascular magnetic resonance angiography of the pulmonary veins. *J Cardiovasc Magn R* 2020;**22**:78.
21. Ginami G, Lopez K, Mukherjee RK, Neji R, Munoz C, Roujol S *et al.* Non-contrast enhanced simultaneous 3D whole-heart bright-blood pulmonary veins visualization and black-blood quantification of atrial wall thickness. *Magn Reson Med* 2019;**81**:1066–79.
22. Bisbal F, Gomez-Pulido F, Cabanas-Grandio P, Akoum N, Calvo M, Andreu D *et al.* Left atrial geometry improves risk prediction of thromboembolic events in patients with atrial fibrillation. *J Cardiovasc Electrophysiol* 2016;**27**:804–10.
23. Bieging ET, Morris A, Chang L, Dagher L, Marrouche NF, Cates J. Statistical shape analysis of the left atrial appendage predicts stroke in atrial fibrillation. *Int J Cardiovas Imag* 2021;**37**:2521–7.
24. Di Biase L, Santangeli P, Anselmino M, Mohanty P, Salvetti I, Gili S *et al.* Does the left atrial appendage morphology correlate with the risk of stroke in patients with atrial fibrillation? Results from a multicenter study. *J Am Coll Cardiol* 2012;**60**:531–8.
25. Khurram IM, Dewire J, Mager M, Maqbool F, Zimmerman SL, Zipunnikov V *et al.* Relationship between left atrial appendage morphology and stroke in patients with atrial fibrillation. *Heart Rhythm* 2013;**10**:1843–9.
26. Yaghi S, Chang AD, Akiki R, Collins S, Novack T, Hemendinger M *et al.* The left atrial appendage morphology is associated with embolic stroke subtypes using a simple classification system: a proof of concept study. *J Cardiovasc Comput Tomogr* 2020;**14**:27–33.
27. Hof I, Chilukuri K, Arbab-Zadeh A, Scherr D, Dalal D, Nazarian S *et al.* Does left atrial volume and pulmonary venous anatomy predict the outcome of catheter ablation of atrial fibrillation? *J Cardiovasc Electrophysiol* 2009;**20**:1005–10.
28. Gonzales RA, Seemann F, Lamy J, Arvidsson PM, Heiberg E, Murray V *et al.* Automated left atrial time-resolved segmentation in MRI long-axis cine images using active contours. *BMC Med Imaging* 2021;**21**:101.
29. Zhang X, Noga M, Martin DG, Punithakumar K. Fully automated left atrium segmentation from anatomical cine long-axis MRI sequences using deep convolutional neural network with unscented Kalman filter. *Med Image Anal* 2021;**68**:101916.
30. Ahtarovski KA, Iversen KK, Lonborg JT, Madsen PL, Engstrom T, Vejlstrup N. Left atrial and ventricular function during dobutamine and glycopyrrolate stress in healthy young and elderly as evaluated by cardiac magnetic resonance. *Am J Physiol Heart Circ Physiol* 2012;**303**:H1469–73.
31. Le Ven F, Bibeau K, De Larochelliere E, Tizon-Marcos H, Deneault-Bissonnette S, Pibarot P *et al.* Cardiac morphology and function reference values derived from a large subset of healthy young Caucasian adults by magnetic resonance imaging. *Eur Heart J Cardiovasc Imaging* 2016;**17**:981–90.
32. Li WH, Wan K, Han YC, Liu H, Cheng W, Sun JY *et al.* Reference value of left and right atrial size and phasic function by SSFP CMR at 3.0T in healthy Chinese adults. *Sci Rep* 2017;**7**:3196.
33. Nacif MS, Barranhas AD, Turkbey E, Marchiori E, Kawel N, Mello RAF *et al.* Left atrial volume quantification using cardiac MRI in atrial fibrillation: comparison of the Simpson's method with biplane area-length, ellipse, and three-dimensional methods. *Diagn Interv Radiol* 2013;**19**:213–20.
34. Lang RM, Bierig M, Devereux RB, Flachskampf FA, Foster E, Pellikka PA *et al.*; European Association of Echocardiography. Recommendations for chamber quantification: a report from the American Society of Echocardiography's guidelines and standards committee and the chamber quantification writing group, developed in conjunction with the European Association of Echocardiography, a branch of the European Society of Cardiology. *J Am Soc Echocardiogr* 2005;**18**:1440–63.
35. Kawel-Boehm N, Hetzel SJ, Ambale-Venkatesh B, Captur G, Francois CJ, Jerosch-Herold M *et al.* Reference ranges ("normal values") for cardiovascular magnetic resonance (CMR) in adults and children: 2020 update. *J Cardiovasc Magn Reson* 2020;**22**:87.
36. Maceira AM, Cosin-Sales J, Roughton M, Prasad SK, Pennell DJ. Reference left atrial dimensions and volumes by steady state free precession cardiovascular magnetic resonance. *J Cardiovasc Magn Reson* 2010;**12**:65.
37. Kowallick JT, Kutty S, Edelmann F, Chiribiri A, Villa A, Steinmetz M *et al.* Quantification of left atrial strain and strain rate using cardiovascular magnetic resonance myocardial feature tracking: a feasibility study. *J Cardiovasc Magn Reson* 2014;**16**:60.
38. Kramer CM, DiMarco JP, Kolm P, Ho CY, Desai MY, Kwong RY *et al.* Predictors of major atrial fibrillation endpoints in the National Heart, Lung, and Blood Institute HCMR. *JACC Clin Electrophysiol* 2021;doi: 10.1016/j.jacep.2021.04.004.
39. Pellicori P, Zhang JF, Lukaschuk E, Joseph AC, Bourantas CV, Loh H *et al.* Left atrial function measured by cardiac magnetic resonance imaging in patients with heart failure: clinical associations and prognostic value. *Eur Heart J* 2015;**36**:733–42.
40. Funk S, Kermer J, Doganguezel S, Schwenke C, von Knobelsdorff-Brenkenhoff F, Schulz-Menger J. Quantification of the left atrium applying cardiovascular magnetic resonance in clinical routine. *Scand Cardiovasc J* 2018;**52**:85–92.
41. Imai M, Ambale Venkatesh B, Samiei S, Donekal S, Habibi M, Armstrong AC *et al.* Multi-ethnic study of atherosclerosis: association between left atrial function using tissue tracking from cine MR imaging and myocardial fibrosis. *Radiology* 2014;**273**:703–13.
42. Evin M, Redheuil A, Soulat G, Perdrix L, Ashrafpoor G, Giron A *et al.* Left atrial aging: a cardiac magnetic resonance feature-tracking study. *Am J Physiol Heart Circ Physiol* 2016;**310**:H542–9.
43. Tagare HD. Shape-based nonrigid correspondence with application to heart motion analysis. *IEEE Trans Med Imaging* 1999;**18**:570–9.
44. Papademetris X, Sinusas AJ, Dione DP, Duncan JS. Estimation of 3D left ventricular deformation from echocardiography. *Med Image Anal* 2001;**5**:17–28.
45. Schneider C, Malisius R, Krause K, Lampe F, Bahlmann E, Boczor S *et al.* Strain rate imaging for functional quantification of the left atrium: atrial deformation predicts the maintenance of sinus rhythm after catheter ablation of atrial fibrillation. *Eur Heart J* 2008;**29**:1397–409.
46. Cameli M, Caputo M, Mondillo S, Ballo P, Palmerini E, Lisi M *et al.* Feasibility and reference values of left atrial longitudinal strain imaging by two-dimensional speckle tracking. *Cardiovasc Ultrasound* 2009;**7**:6.
47. Hor KN, Gottliebson WM, Carson C, Wash E, Cnota J, Fleck R *et al.* Comparison of magnetic resonance feature tracking for strain calculation with harmonic phase imaging analysis. *JACC Cardiovasc Imaging* 2010;**3**:144–51.
48. Hor KN, Baumann R, Pedrizzetti G, Tonti G, Gottliebson WM, Taylor M *et al.* Magnetic resonance derived myocardial strain assessment using feature tracking. *J Vis Exp* 2011;**48**:2356.
49. Habibi M, Chahal H, Opdahl A, Gjesdal O, Helle-Valle TM, Heckbert SR *et al.* Association of CMR-measured LA function with heart failure development: results from the MESA study. *JACC Cardiovasc Imaging* 2014;**7**:570–9.
50. Evin M, Cluzel P, Lamy J, Rosenbaum D, Kusmia S, Defrance C *et al.* Assessment of left atrial function by MRI myocardial feature tracking. *J Magn Reson Imaging* 2015;**42**:379–89.

51. Lamy J, Soulat G, Evin M, Huber A, de Cesare A, Giron A *et al.* Scan-rescan reproducibility of ventricular and atrial MRI feature tracking strain. *Comput Biol Med* 2018;**92**:197–203.
52. Morais P, Marchi A, Bogaert JA, Dresselaers T, Heyde B, D'hooge J *et al.* Cardiovascular magnetic resonance myocardial feature tracking using a non-rigid, elastic image registration algorithm: assessment of variability in a real-life clinical setting. *J Cardiovasc Magn Reson* 2017;**19**:24.
53. Hu CX, Parulji N, Lu H, Papademetris X, Duncan JS, Peters DC. 3D left atrial strain imaging based on multi-slice radial cine and feature tracking. In: *ISMRM*. Honolulu, HI, USA, 2017, 2876.
54. Varela M, Queiros S, Anjari M, Correia T, King AP, Bharath AA *et al.* Strain maps of the left atrium imaged with a novel high-resolution CINE MRI protocol. *IEEE Eng Med Bio* 2020;1178–81.
55. Sun BJ, Park J-H, Lee M, Choi J-O, Lee J-H, Shin M-S *et al.* Normal reference values for left atrial strain and its determinants from a large Korean Multicenter Registry. *J Cardiovasc Imaging* 2020;**28**:186–98.
56. Doria de Vasconcellos H, Win TT, Chamera E, Hong SY, Venkatesh BA, Young P *et al.* References values for left atrial volumes, emptying fractions, strains, and strain rates and their determinants by age, gender, and ethnicity: the Multiethnic Study of Atherosclerosis (MESA). *Acad Radiol* 2021;**28**:356–63.
57. Peng JP, Zhao XD, Zhao L, Fan ZM, Wang Z, Chen H *et al.* Normal values of myocardial deformation assessed by cardiovascular magnetic resonance feature tracking in a healthy Chinese population: a multicenter study. *Front Physiol* 2018;**9**:1181.
58. Hoit BD. Left atrial remodeling: more than just left atrial enlargement. *Circ Cardiovasc Imaging* 2017;**10**:e006036.
59. Inoue YY, Alissa A, Khurram IM, Fukumoto K, Habibi M, Venkatesh BA *et al.* Quantitative tissue-tracking cardiac magnetic resonance (CMR) of left atrial deformation and the risk of stroke in patients with atrial fibrillation. *J Am Heart Assoc* 2015;**4**:e001844.
60. Markman TM, Habibi M, Venkatesh BA, Zareian M, Wu C, Heckbert SR *et al.* Association of left atrial structure and function and incident cardiovascular disease in patients with diabetes mellitus: results from multi-ethnic study of atherosclerosis (MESA). *Eur Heart J Cardiovasc Imaging* 2017;**18**:1138–44.
61. Singh A, Addetia K, Maffessanti F, Mor-Avi V, Lang RM. LA strain for categorization of LV diastolic dysfunction. *JACC Cardiovasc Imaging* 2017;**10**:735–43.
62. Cameli M, Lisi M, Focardi M, Reccia R, Natali BM, Sparla S *et al.* Left atrial deformation analysis by speckle tracking echocardiography for prediction of cardiovascular outcomes. *Am J Cardiol* 2012;**110**:264–9.
63. Chirinos JA, Sardana M, Ansari B, Satija V, Kuriakose D, Edelstein I *et al.* Left atrial phasic function by cardiac magnetic resonance feature tracking is a strong predictor of incident cardiovascular events. *Circ Cardiovasc Imaging* 2018;**11**:e007512.
64. Modin D, Biering-Sorensen SR, Mogelvang R, Alhakak AS, Jensen JS, Biering ST. Prognostic value of left atrial strain in predicting cardiovascular morbidity and mortality in the general population. *Eur Heart J Cardiovasc Imaging* 2019;**20**:804–15.
65. Mondillo S, Cameli M, Caputo ML, Lisi M, Palmerini E, Padeletti M *et al.* Early detection of left atrial strain abnormalities by speckle-tracking in hypertensive and diabetic patients with normal left atrial size. *J Am Soc Echocardiog* 2011;**24**:898–908.
66. Sahebjam M, Mazareei A, Lotfi-Tokaldany M, Ghaffari N, Zoroufian A, Sheikhfatollahi M. Comparison of left atrial function between hypertensive patients with normal atrial size and normotensive subjects using strain rate imaging technique. *Arch Cardiovasc Imaging* 2014;**2**:
67. Hennawy B, El Kilany W, Galal H, Mamdouh A. Role of speckle tracking echocardiography in detecting early left atrial dysfunction in hypertensive patients. *Egypt Heart J* 2018;**70**:217–23.
68. Evin M, Broadhouse KM, Callaghan FM, McGrath RT, Glastras S, Kozor R *et al.* Impact of obesity and epicardial fat on early left atrial dysfunction assessed by cardiac MRI strain analysis. *Cardiovasc Diabetol* 2016;**15**:164.
69. Sarvari SI, Haugaa KH, Stokke TM, Ansari HZ, Leren IS, Hegbom F *et al.* Strain echocardiographic assessment of left atrial function predicts recurrence of atrial fibrillation. *Eur Heart J Cardiovasc Imaging* 2016;**17**:660–7.
70. Habibi M, Lima JAC, Ipek EG, Zimmerman SL, Zipunnikov V, Spragg D *et al.* The association of baseline left atrial structure and function measured with cardiac magnetic resonance and pulmonary vein isolation outcome in patients with drug-refractory atrial fibrillation. *Heart Rhythm* 2016;**13**:1037–44.
71. Cameli M, Lisi M, Reccia R, Bennati E, Malandrino A, Solari M *et al.* Pre-operative left atrial strain predicts post-operative atrial fibrillation in patients undergoing aortic valve replacement for aortic stenosis. *Int J Cardiovasc Imaging* 2014;**30**:279–86.
72. Cameli M, Pastore MC, Mandoli GE. Left atrial strain: a key element for the evaluation of patients with HFpEF. *Int J Cardiol* 2021;**323**:197–8.
73. Thomas L, Marwick TH, Popescu BA, Donal E, Badano LP. Left atrial structure and function, and left ventricular diastolic dysfunction: JACC state-of-the-art review. *J Am Coll Cardiol* 2019;**73**:1961–77.
74. Cameli M, Lisi M, Righini FM, Massoni A, Natali BM, Focardi M *et al.* Usefulness of atrial deformation analysis to predict left atrial fibrosis and endocardial thickness in patients undergoing mitral valve operations for severe mitral regurgitation secondary to mitral valve prolapse. *Am J Cardiol* 2013;**111**:595–601.
75. Huber A, Lamy J, Rahhal A, Evin M, Atassi F, Defrance C *et al.* Cardiac MR Strain: A Noninvasive Biomarker of Fibrofatty Remodeling of the Left Atrial Myocardium. *Radiology* 2018;**286**:83–92. doi: 10.1148/radiol.2017162787.
76. Kuppahally SS, Akoum N, Burgon NS, Badger TJ, Kholmovski EG, Vijayakumar S *et al.* Left atrial strain and strain rate in patients with paroxysmal and persistent atrial fibrillation. *Circ Cardiovasc Imaging* 2010;**3**:231–9.
77. Peters DC, Duncan JS, Grunseich K, Marieb MA, Cornfeld D, Sinusas AJ *et al.* CMR-verified lower LA strain in the presence of regional atrial fibrosis in atrial fibrillation. *JACC Cardiovasc Imaging* 2017;**10**:207–8.
78. Genovese D, Singh A, Volpato V, Kruse E, Weinert L, Yamat M *et al.* Load dependency of left atrial strain in normal subjects. *J Am Soc Echocardiog* 2018;**31**:1221–8.
79. Chirinos JA, Sardana M, Satija V, Gillebert TC, De Buyzere ML, Chahwala J *et al.* Effect of obesity on left atrial strain in persons aged 35–55 years (The Asklepios Study). *Am J Cardiology* 2019;**123**:854–61.
80. Bertelsen L, Diederichsen SZ, Haugan KJ, Brandes A, Graff C, Krieger D *et al.* Left atrial volume and function assessed by cardiac magnetic resonance imaging are markers of subclinical atrial fibrillation as detected by continuous monitoring. *Europace* 2020;**22**:724–31.
81. Zareian M, Ciuffo L, Habibi M, Opdahl A, Chamera EH, Wu CO *et al.* Left atrial structure and functional quantitation using cardiovascular magnetic resonance and multimodality tissue tracking: validation and reproducibility assessment. *J Cardiovasc Magn Reson* 2015;**17**:52.
82. Kowallick JT, Morton G, Lamata P, Jogiya R, Kutty S, Hasenfuß G *et al.* Quantification of atrial dynamics using cardiovascular magnetic resonance: inter-study reproducibility. *J Cardiovasc Magn Reson* 2015;**17**:36.
83. Truong VT, Palmer C, Wolking S, Sheets B, Young M, Ngo TNM *et al.* Normal left atrial strain and strain rate using cardiac magnetic resonance feature tracking in healthy volunteers. *Eur Heart J Cardiovasc Imaging* 2020;**21**:446–53.
84. Pathan F, Zainal Abidin HA, Vo QH, Zhou H, D'Angelo T, Elen E *et al.* Left atrial strain: a multi-modality, multi-vendor comparison study. *Eur Heart J Cardiovasc Imaging* 2021;**22**:102–10.
85. Farsalinos KE, Daraban AM, Ünlü S, Thomas JD, Badano LP, Voigt J-U. Head-to-head comparison of global longitudinal strain measurements among nine different vendors: the EACVI/ASE inter-vendor comparison study. *J Am Soc Echocardiog* 2015;**28**:1171–81.e2.
86. Backhaus SJ, Metschies G, Billing M, Schmidt-Rimpler J, Kowallick JT, Gertz RJ *et al.* Defining the optimal temporal and spatial resolution for cardiovascular magnetic resonance imaging feature tracking. *J Cardiovasc Magn Reson* 2021;**23**:60.
87. Voigt J-U, Mălăescu G-G, Haugaa K, Badano L. How to do LA strain. *Eur Heart J Cardiovasc Imaging* 2020;**21**:715–7.
88. Nabeshima Y, Kitano T, Takeuchi M. Reliability of left atrial strain reference values: a 3D echocardiographic study. *PLos One* 2021;**16**:e0250089.
89. Thiedemann KU, Ferrans VJ. Left atrial ultrastructure in mitral valvular disease. *Am J Pathol* 1977;**89**:575–604.
90. Steiner I, Hajkova P, Kvasnicka J, Kholova I. Myocardial sleeves of pulmonary veins and atrial fibrillation: a postmortem histopathological study of 100 subjects. *Virchows Arch* 2006;**449**:88–95.
91. Latif SR, Nguyen VQ, Peters DC, Soufer A, Henry ML, Grunseich K *et al.* Left atrial fibrosis correlates with extent of left ventricular myocardial delayed enhancement and left ventricular strain in hypertrophic cardiomyopathy. *Int J Cardiovasc Imaging* 2019;**35**:1309–18.
92. de Oliveira IM, Oliveira BD, Scanavacca MI, Gutierrez PS. Fibrosis, myocardial crossings, disconnections, abrupt turns, and epicardial reflections: do they play an actual role in human permanent atrial fibrillation? A controlled necropsy study. *Cardiovasc Pathol* 2013;**22**:65–9.
93. Cochet H, Komatsu Y, Sacher F, Jadidi AS, Scherr D, Riffaud M *et al.* Integration of merged delayed-enhanced magnetic resonance imaging and multidetector computed tomography for the guidance of ventricular tachycardia ablation: a pilot study. *J Cardiovasc Electrophysiol* 2013;**24**:419–26.
94. Quail M, Grunseich K, Baldassarre LA, Mojibian H, Marieb MA, Cornfeld D *et al.* Prognostic and functional implications of left atrial late gadolinium enhancement cardiovascular magnetic resonance. *J Cardiovasc Magn Reson* 2019;**21**:2.
95. Nattel S, Burstein B, Dobrev D. Atrial remodeling and atrial fibrillation mechanisms and implications. *Circ Arrhythm Electrophysiol* 2008;**1**:62–73.
96. Verma A, Wazni OM, Marrouche NF, Martin DO, Kilicaslan F, Minor S *et al.* Pre-existent left atrial scarring in patients undergoing pulmonary vein antrum isolation: an independent predictor of procedural failure. *J Am Coll Cardiol* 2005;**45**:285–92.

97. Simonetti OP, Kim RJ, Fieno DS, Hillenbrand HB, Wu E, Bundy JM *et al.* An improved MR imaging technique for the visualization of myocardial infarction. *Radiology* 2001;**218**:215–23.
98. Kim RJ, Fieno DS, Parrish TB, Harris K, Chen EL, Simonetti O *et al.* Relationship of MRI delayed contrast enhancement to irreversible injury, infarct age, and contractile function. *Circulation* 1999;**100**:1992–2002.
99. Peters DC, Wylie JV, Hauser TH, Kissinger KV, Botnar RM, Essebag V *et al.* Detection of pulmonary vein and left atrial scar after catheter ablation with three-dimensional navigator-gated delayed enhancement MR imaging: initial experience. *Radiology* 2007;**243**:690–5.
100. Rosen BR, Belliveau JW, Vevea JM, Brady TJ. Perfusion imaging with NMR contrast agents. *Magn Reson Med* 1990;**14**:249–65.
101. Cui Y, Cao YK, Song J, Dong NG, Kong XC, Wang J *et al.* Association between myocardial extracellular volume and strain analysis through cardiovascular magnetic resonance with histological myocardial fibrosis in patients awaiting heart transplantation. *J Cardiovasc Magn Reson* 2018;**20**:25.
102. Platonov PG, Ivanov V, Ho SY, Mitrofanova L. Left atrial posterior wall thickness in patients with and without atrial fibrillation: data from 298 consecutive autopsies. *J Cardiovasc Electrophysiol* 2008;**19**:689–92.
103. Kellman P, Arai AE, McVeigh ER, Aletras AH. Phase-sensitive inversion recovery for detecting myocardial infarction using gadolinium-delayed hyperenhancement. *Magn Reson Med* 2002;**47**:372–83.
104. Hu CX, Huber S, Latif SR, Santacana-Laffitte G, Mojibian HR, Baldassarre LA *et al.* REPAIRit: improving myocardial nulling and ghosting artifacts of 3D navigator-gated late gadolinium enhancement imaging during arrhythmia. *J Magn Reson Imaging* 2019;**49**:688–99.
105. Lee S, Schär M, Kozerke S, Harouni A, Sena-Weltin V, Zviman MM *et al.* Independent respiratory navigators for improved 3D PSIR imaging of myocardial infarctions. *J Cardiovasc Magn Reson* 2011;**13**:P18.
106. Klein C, Nekolla SG, Balbach T, Schnackenburg B, Nagel E, Fleck E *et al.* The influence of myocardial blood flow and volume of distribution on late Gd-DTPA kinetics in ischemic heart failure. *J Magn Reson Imaging* 2004;**20**:588–93.
107. Siebermair J, Kholmovski EG, Marrouche N. Assessment of left atrial fibrosis by late gadolinium enhancement magnetic resonance imaging: methodology and clinical implications. *JACC Clin Electrophysiol* 2017;**3**:791–802.
108. Holtackers RJ, Van De Heyning CM, Nazir MS, Rashid I, Ntalas I, Rahman H *et al.* Clinical value of dark-blood late gadolinium enhancement cardiovascular magnetic resonance without additional magnetization preparation. *J Cardiovasc Magn Reson* 2019;**21**:44
109. PPeel SA, Morton G, Chiribiri A, Schuster A, Nagel E, Botnar RM. Dual inversion-recovery mr imaging sequence for reduced blood signal on late gadolinium-enhanced images of myocardial scar. Radiology. 2012 **264**:242–9. doi: 10.1148/radiol.12112004.
110. Moghari MH, Peters DC, Smink J, Goepfert L, Kissinger KV, Goddu B *et al.* Pulmonary vein inflow artifact reduction for free-breathing left atrium late gadolinium enhancement. *Magn Reson Med* 2011;**66**:180–6.
111. Henningsson M, Carlhall CJ. Inflow artifact reduction using an adaptive flip-angle navigator restore pulse for late gadolinium enhancement of the left atrium. *Magn Reson Med* 2020;**84**:3308–15.
112. Peters DC, Shaw JL, Knowles BR, Moghari MH, Manning WJ. Respiratory bellows-gated late gadolinium enhancement of the left atrium. *J Magn Reson Imaging* 2013;**38**:1210–4.
113. Wong CX, Abed HS, Molaee P, Nelson AJ, Brooks AG, Sharma G *et al.* Pericardial fat is associated with atrial fibrillation severity and ablation outcome. *J Am Coll Cardiol* 2011;**57**:1745–51.
114. Armour JA, Murphy DA, Yuan BX, MacDonald S, Hopkins DA. Gross and microscopic anatomy of the human intrinsic cardiac nervous system. *Anat Rec* 1997;**247**:289–98.
115. Rehwald W, Jensen CJ, Jenista E, Darty S, Spatz D, Kim RJ. Highly effective fat suppression in clinical T1-weighted imaging of ischemic and non-ischemic heart disease with DeSPAIR. *J Cardiovasc Magn Reson* 2012;**14**:O53.
116. Shaw J, Knowles B, Goldfarb J, Manning W, Peters D. Left atrial late gadolinium enhancement with water-fat separation: the importance of phase-encoding order. *J Magn Reson Imaging* 2014;**40**:119–25.
117. Keegan J, Gatehouse PD, Haldar S, Wage R, Babu-Narayan SV, Firmin DN. Dynamic inversion time for improved 3D late gadolinium enhancement imaging in patients with atrial fibrillation. *Magn Reson Med* 2015;**73**:646–54.
118. Weingartner S, Akcakaya M, Basha T, Kissinger KV, Goddu B, Berg S *et al.* Combined saturation/inversion recovery sequences for improved evaluation of scar and diffuse fibrosis in patients with arrhythmia or heart rate variability. *Magn Reson Med* 2014;**71**:1024–34.
119. Menon RG, Miller GW, Jeudy J, Rajagopalan S, Shin T. Free breathing three-dimensional late gadolinium enhancement cardiovascular magnetic resonance using outer volume suppressed projection navigators. *Magn Reson Med* 2017;**77**:1533–43.
120. Neilan TG, Mongeon FP, Shah RV, Coelho O, Abbasi SA, Dodson JA *et al.* Myocardial extracellular volume expansion and the risk of recurrent atrial fibrillation after pulmonary vein isolation. *JACC Cardiovasc Imaging* 2014;**7**:1–11.
121. Chubb H, Aziz S, Karim R, Sohns C, Razeghi O, Williams SE *et al.* Optimization of late gadolinium enhancement cardiovascular magnetic resonance imaging of post-ablation atrial scar: a cross-over study. *J Cardiovasc Magn Reson* 2018;**20**:30.
122. Knowles BR, Peters DC, Clough RE, Razavi R, Schaeffter T, Prieto C. Three-dimensional late gadolinium-enhanced MR imaging of the left atrium: a comparison of spiral versus Cartesian k-space trajectories. *J Magn Reson Imaging* 2014;**39**:211–6.
123. Akcakaya M, Rayatzadeh H, Basha TA, Hong SN, Chan RH, Kissinger KV *et al.* Accelerated late gadolinium enhancement cardiac MR imaging with isotropic spatial resolution using compressed sensing: initial experience. *Radiology* 2012;**264**:691–9.
124. Basha TA, Akcakaya M, Liew C, Tsao CW, Delling FN, Addae G *et al.* Clinical performance of high-resolution late gadolinium enhancement imaging with compressed sensing. *J Magn Reson Imaging* 2017;**46**:1829–38.
125. McGann CJ, Kholmovski EG, Oakes RS, Blauer JJ, Daccarett M, Segerson N *et al.* New magnetic resonance imaging-based method for defining the extent of left atrial wall injury after the ablation of atrial fibrillation. *J Am Coll Cardiol* 2008;**52**:1263–71.
126. Badger TJ, Oakes RS, Daccarett M, Burgon NS, Akoum N, Fish EN *et al.* Temporal left atrial lesion formation after ablation of atrial fibrillation. *Heart Rhythm* 2009;**6**:161–8.
127. Malcolme-Lawes LC, Juli C, Karim R, Bai W, Quest R, Lim PB *et al.* Automated analysis of atrial late gadolinium enhancement imaging that correlates with endocardial voltage and clinical outcomes: a 2-center study. *Heart Rhythm* 2013;**10**:1184–91.
128. Peters DC, Wylie J, Hauser T, Nezafat R, Han Y, Woo J *et al.* Recurrence of atrial fibrillation correlated with extent of post-procedural left atrial late gadolinium enhancement: implications for the right inferior pulmonary vein. *JACC Cardiovasc Imaging* 2009;**2**:308–16.
129. Chubb H, Karim R, Roujol S, Nunez-Garcia M, Williams SE, Whitaker J *et al.* The reproducibility of late gadolinium enhancement cardiovascular magnetic resonance imaging of post-ablation atrial scar: a cross-over study. *J Cardiovasc Magn Reson* 2018;**20**:21.
130. Andreu D, Gomez-Pulido F, Calvo M, Carlosena-Remirez A, Bisbal F, Borras R *et al.* Contact force threshold for permanent lesion formation in atrial fibrillation ablation: a cardiac magnetic resonance-based study to detect ablation gaps. *Heart Rhythm* 2016;**13**:37–45.
131. Al Jefairi N, Camaioni C, Sridi S, Cheniti G, Takigawa M, Nivet H *et al.* Relationship between atrial scar on cardiac magnetic resonance and pulmonary vein reconnection after catheter ablation for paroxysmal atrial fibrillation. *J Cardiovasc Electrophysiol* 2019;**30**:727–40.
132. Bishop M, Rajani R, Plank G, Gaddum N, Carr-White G, Wright M *et al.* Three-dimensional atrial wall thickness maps to inform catheter ablation procedures for atrial fibrillation. *Europace* 2016;**18**:376–83.
133. Chrispin J, Ipek EG, Habibi M, Yang E, Spragg D, Marine JE *et al.* Clinical predictors of cardiac magnetic resonance late gadolinium enhancement in patients with atrial fibrillation. *Europace* 2017;**19**:371–7.
134. Kholmovski EG, Silvernagel J, Angel N, Vijayakumar S, Thomas S, Dosdall D *et al.* Acute noncontrast T1-weighted magnetic resonance imaging predicts chronic radiofrequency ablation lesions. *J Cardiovasc Electrophysiol* 2018;**29**:1556–62.
135. Vergara GR, Vijayakumar S, Kholmovski EG, Blauer JJ, Guttman MA, Gloschat C *et al.* Real-time magnetic resonance imaging-guided radiofrequency atrial ablation and visualization of lesion formation at 3 Tesla. *Heart Rhythm* 2011;**8**:295–303.
136. Guttman MA, Tao S, Fink S, Tunin R, Schmidt EJ, Herzka DA *et al.* Acute enhancement of necrotic radio-frequency ablation lesions in left atrium and pulmonary vein ostia in swine model with non-contrast-enhanced T-1-weighted MRI. *Magn Reson Med* 2020;**83**:1368–79.
137. Hsing J, Peters DC, Knowles BR, Manning WJ, Josephson ME. Cardiovascular magnetic resonance imaging of scar development following pulmonary vein isolation: a prospective study. *PLoS One* 2014;**9**:e104844. doi: 10.1371/journal.pone.0104844.
138. Oakes R, Kholmovski E, DiBella E, Segerson N, Fish E, McGann C *et al.* (eds). *Application of DE-MRI to Assess LA Myocardium Composition in AF Patients*. Toronto, CA: International Society of Magnetic Resonance in Medicine, 2008.
139. Mahnkopf C, Badger TJ, Burgon NS, Daccarett M, Haslam TS, Badger CT *et al.* Evaluation of the left atrial substrate in patients with lone atrial fibrillation using delayed-enhanced MRI: implications for disease progression and response to catheter ablation. *Heart Rhythm* 2010;**7**:1475–81.

140. McGann C, Akoum N, Patel A, Kholmovski E, Revelo P, Damal K *et al.* Atrial fibrillation ablation outcome is predicted by left atrial remodeling on MRI. *Circ Arrhythm Electrophysiol* 2014;**7**:23–30.
141. Marrouche NF, Wilber D, Hindricks G, Jais P, Akoum N, Marchlinski F *et al.* Association of atrial tissue fibrosis identified by delayed enhancement MRI and atrial fibrillation catheter ablation: the DECAAF study. *JAMA* 2014;**311**:498–506.
142. Marrouche NF, Greene T, Dean JM, Kholmovski EG, Morrison-de Boer L, Mansour M *et al.*; DECAAF II Investigators. Efficacy of LGE-MRI-guided fibrosis ablation versus conventional catheter ablation of atrial fibrillation: the DECAAF II trial: study design. *J Cardiovasc Electrophysiol* 2021;**32**:916–24.
143. Roh SY, Lee DI, Hwang SH, Lee KN, Baek YS, Iqbal M *et al.* Association of left atrial pressure with late gadolinium enhancement extent in patient who underwent catheter ablation for atrial fibrillation. *Sci Rep* 2020;**10**:16486.
144. Ghafouri K, Franke KB, Foo FS, Stiles MK. Clinical utility of cardiac magnetic resonance imaging to assess the left atrium before catheter ablation for atrial fibrillation—a systematic review and meta-analysis. *Int J Cardiol* 2021;**339**:192–202.
145. Gonzales MJ, Vincent KP, Rappel WJ, Narayan SM, McCulloch AD. Structural contributions to fibrillatory rotors in a patient-derived computational model of the atria. *Europace* 2014;**16**:iv3–10.
146. Roy A, Varela M, Chubb H, MacLeod R, Hancox JC, Schaeffter T *et al.* Identifying locations of re-entrant drivers from patient-specific distribution of fibrosis in the left atrium. *Plos Comput Biol* 2020;**16**:e1008086.
147. Sohns C, Lemes C, Metzner A, Fink T, Chmelevsky M, Maurer T *et al.* First-in-man analysis of the relationship between electrical rotors from noninvasive panoramic mapping and atrial fibrosis from magnetic resonance imaging in patients with persistent atrial fibrillation. *Circ Arrhythm Electrophysiol* 2017;**10**:e004419.
148. Chrispin J, Ipek EG, Zahid S, Prakosa A, Habibi M, Spragg D *et al.* Lack of regional association between atrial late gadolinium enhancement on cardiac magnetic resonance and atrial fibrillation rotors. *Heart Rhythm* 2016;**13**:654–60.
149. Daccarett M, Badger TJ, Akoum N, Burgon NS, Mahnkopf C, Vergara G *et al.* Association of left atrial fibrosis detected by delayed-enhancement magnetic resonance imaging and the risk of stroke in patients with atrial fibrillation. *J Am Coll Cardiol* 2011;**57**:831–8.
150. King JB, Azadani PN, Suksaranjit P, Bress AP, Witt DM, Han FT *et al.* Left atrial fibrosis and risk of cerebrovascular and cardiovascular events in patients with atrial fibrillation. *J Am Coll Cardiol* 2017;**70**:1311–21.
151. Goette A, Kalman JM, Aguinaga L, Akar J, Cabrera JA, Chen SA *et al.* EHRA/HRS/APHRS/SOLAECE expert consensus on atrial cardiomyopathies: definition, characterization, and clinical implication. *Heart Rhythm* 2017;**14**:E3–40.
152. Kamel H, Okin PM, Longstreth WT, Elkind MSV, Soliman EZ. Atrial cardiopathy: a broadened concept of left atrial thromboembolism beyond atrial fibrillation. *Future Cardiol* 2015;**11**:323–31.
153. Siebermair J, Suksaranjit P, McGann CJ, Peterson KA, Kheirkhahan M, Baher AA *et al.* Atrial fibrosis in non-atrial fibrillation individuals and prediction of atrial fibrillation by use of late gadolinium enhancement magnetic resonance imaging. *J Cardiovasc Electrophysiol* 2019;**30**:550–6.
154. Barbhaiya CR, Kumar S, Baldinger SH, Michaud GF, Stevenson WG, Falk R *et al.* Electrophysiologic assessment of conduction abnormalities and atrial arrhythmias associated with amyloid cardiomyopathy. *Heart Rhythm* 2016;**13**:383–90.
155. Wijffels MCEF, Kirchhof CJHJ, Dorland R, Allessie MA. Atrial-fibrillation begets atrial-fibrillation—a study in awake chronically instrumented goats. *Circulation* 1995;**92**:1954–68.
156. Seemann F, Baldassarre LA, Llanos-Chea F, Gonzales RA, Grunseich K, Hu CX *et al.* Assessment of diastolic function and atrial remodeling by MRI—validation and correlation with echocardiography and filling pressure. *Physiol Rep* 2018;**6**:e13828.
157. Bertelsen L, Diederichsen SZ, Haugan KJ, Brandes A, Graff C, Krieger D *et al.* Left atrial late gadolinium enhancement is associated with incident atrial fibrillation as detected by continuous monitoring with implantable loop recorders. *JACC Cardiovasc Imaging* 2020;**13**:1690–700.
158. Dagher L, Shi HY, Zhao Y, Mitlacher M, Schnupp S, Ajmi I *et al.* Atrial fibrosis progression in patients with no history of atrial fibrillation. *J Cardiovasc Electrophysiol* 2021;**32**:2140–7.
159. Jana S, Hu M, Shen MC, Kassiri Z. Extracellular matrix, regional heterogeneity of the aorta, and aortic aneurysm. *Exp Mol Med* 2019; **51**:1.
160. McCarthy KP, Ring L, Rana BS. Anatomy of the mitral valve: understanding the mitral valve complex in mitral regurgitation. *Eur J Echocardiogr* 2010;**11**:I3–9.
161. Cochet H, Mouries A, Nivet H, Sacher F, Derval N, Denis A *et al.* Age, atrial fibrillation, and structural heart disease are the main determinants of left atrial fibrosis detected by delayed-enhanced magnetic resonance imaging in a general cardiology population. *J Cardiovasc Electrophysiol* 2015;**26**:484–92.
162. Bertelsen L, Alarcon F, Andreasen L, Benito E, Olesen MS, Vejlstrup N *et al.* Verification of threshold for image intensity ratio analyses of late gadolinium enhancement magnetic resonance imaging of left atrial fibrosis in 1.5T scans. *Int J Cardiovasc Imaging* 2020;**36**:513–20.
163. Oakes RS, Badger TJ, Kholmovski EG, Akoum N, Burgon NS, Fish EN *et al.* Detection and quantification of left atrial structural remodeling with delayed-enhancement magnetic resonance imaging in patients with atrial fibrillation. *Circulation* 2009;**119**:1758–67.
164. Khurram IM, Beinart R, Zipunnikov V, Dewire J, Yarmohammadi H, Sasaki T *et al.* Magnetic resonance image intensity ratio, a normalized measure to enable interpatient comparability of left atrial fibrosis. *Heart Rhythm* 2014;**11**:85–92.
165. Kamali R, Schroeder J, DiBella E, Steinberg B, Han FD, Dosdall DJ *et al.* Reproducibility of clinical late gadolinium enhancement magnetic resonance imaging in detecting left atrial scar after atrial fibrillation ablation. *J Cardiovasc Electrophysiol* 2020;**31**:2824–32.
166. Benito EM, Carlosena-Remirez A, Guasch E, Prat-Gonzalez S, Perea RJ, Figueras R *et al.* Left atrial fibrosis quantification by late gadolinium-enhanced magnetic resonance: a new method to standardize the thresholds for reproducibility. *Europace* 2017;**19**:1272–9.
167. Karim R, Housden RJ, Balasubramaniam M, Chen Z, Perry D, Uddin A *et al.* Evaluation of current algorithms for segmentation of scar tissue from late Gadolinium enhancement cardiovascular magnetic resonance of the left atrium: an open-access grand challenge. *J Cardiovasc Magn Reson* 2013;**15**:105.
168. Mărgulescu AD, Nuñez-Garcia M, Alarcón F, Benito EM, Enomoto N, Cozzari J *et al.* Reproducibility and accuracy of late gadolinium enhancement cardiac magnetic resonance measurements for the detection of left atrial fibrosis in patients undergoing atrial fibrillation ablation procedures. *Europace* 2019;**21**:724–31.
169. Harrison JL, Jensen HK, Peel SA, Chiribiri A, Grondal AK, Bloch LO *et al.* Cardiac magnetic resonance and electroanatomical mapping of acute and chronic atrial ablation injury: a histological validation study. *Eur Heart J* 2014;**35**:1486–95.
170. Dewire J, Khurram IM, Pashakhanloo F, Spragg D, Marine JE, Berger RD *et al.* The association of pre-existing left atrial fibrosis with clinical variables in patients referred for catheter ablation of atrial fibrillation. *Clin Med Insights Cardiol* 2014;**8**:25–30.
171. Peters DC, Bertelsen L, Caroline I, Chelikani S. Atrial fibrosis segmentation thresholds: a theoretical and empirical study. *J Cardiovasc Magn Reson* 2016;**18**:P209.
172. Hu CX, Sinusas AJ, Huber S, Thorn S, Stacy MR, Mojibian H *et al.* T1-refBlochi: high resolution 3D post-contrast T1 myocardial mapping based on a single 3D late gadolinium enhancement volume, Bloch equations, and a reference T1. *J Cardiovasc Magn Reson* 2017;**19**:63.
173. Razeghi O, Sim I, Roney CH, Karim R, Chubb H, Whitaker J *et al.* Fully automatic atrial fibrosis assessment using a multilabel convolutional neural network. *Circ Cardiovasc Imaging* 2020;**13**:e011512.
174. Yang G, Zhuang XH, Khan H, Haldar S, Nyktari E, Li L *et al.* Fully automatic segmentation and objective assessment of atrial scars for long-standing persistent atrial fibrillation patients using late gadolinium-enhanced MRI. *Med Phys* 2018;**45**:1562–76.
175. Xiong ZH, Fedorov VV, Fu XH, Cheng E, Macleod R, Zhao JC. Fully automatic left atrium segmentation from late gadolinium enhanced magnetic resonance imaging using a dual fully convolutional neural network. *IEEE Trans Med Imaging* 2019;**38**:515–24.
176. Watson T, Shantsila E, Lip GYH. Mechanisms of thrombogenesis in atrial fibrillation: Virchow's triad revisited. *Lancet* 2009;**373**:155–66.
177. Fyrenius A, Wigstrom L, Ebbers T, Karlsson M, Engvall J, Bolger AF. Three dimensional flow in the human left atrium. *Heart* 2001;**86**:448–55.
178. Markl M, Lee DC, Ng J, Carr M, Carr J, Goldberger JJ. Left atrial 4-dimensional flow magnetic resonance imaging stasis and velocity mapping in patients with atrial fibrillation. *Invest Radiol* 2016;**51**:147–54.
179. Markl M, Lee DC, Furiasse N, Carr M, Foucar C, Ng J *et al.* Left atrial and left atrial appendage 4D blood flow dynamics in atrial fibrillation. *Circ Cardiovasc Imaging* 2016;**9**:e004984.
180. Ma LLN, Yerly JM, Di Sopra L, Piccini D, Lee JS, DiCarlo A *et al.* Using 5D flow MRI to decode the effects of rhythm on left atrial 3D flow dynamics in patients with atrial fibrillation. *Magn Reson Med* 2021;**85**:3125–39.
181. Demirkiran A, Amier RP, Hofman MBM, van der Geest RJ, Robbers LFHJ, Hopman LHGA *et al.* Altered left atrial 4D flow characteristics in patients with paroxysmal atrial fibrillation in the absence of apparent remodeling. *Sci Rep* 2021;**11**:5965.
182. Garcia J, Sheitt H, Bristow MS, Lydell C, Howarth AG, Heydari B *et al.* Left atrial vortex size and velocity distributions by 4D flow MRI in patients with paroxysmal atrial fibrillation: associations with age and CHA2 DS2-VASc risk score. *J Magn Reson Imaging* 2020;**51**:871–84.
183. Spartera M, Pessoa-Amorim G, Stracquadanio A, Von Ende A, Fletcher A, Manley P *et al.* Left atrial 4D flow cardiovascular magnetic resonance: a

reproducibility study in sinus rhythm and atrial fibrillation. *J Cardiovasc Magn Reson* 2021;**23**:29.
184. Pashakhanloo F, Herzka DA, Ashikaga H, Mori S, Gai N, Bluemke DA *et al.* Myofiber architecture of the human atria as revealed by submillimeter diffusion tensor imaging. *Circ Arrhythm Electrophysiol* 2016;**9**:e004133.
185. Coelho-Filho OR, Shah RV, Mitchell R, Neilan TG, Moreno H Jr, Simonson B *et al.* Quantification of cardiomyocyte hypertrophy by cardiac magnetic resonance: implications for early cardiac remodeling. *Circulation* 2013;**128**:1225–33.